

## Phase-factor Dependence of the Geometric Entanglement Measure

Kap Soo JANG, MuSeong KIM and DaeKil PARK\*

Department of Electronic Engineering, Kyungnam University, Changwon 631-701, Korea

(Received 14 January 2011, in final form 17 March 2011)

Any pure three-qubit state is uniquely characterized by one phase and four positive parameters. The geometric measure of entanglement as a function of state parameters can have different expressions that are eigenvalues of the stationarity equations. Each expression has its own applicable domain; thus, the whole state parameter space is divided into subspaces that are ranges of definition for corresponding eigenvalues. These subspaces are invariant under parametrization of states and show the geometry of entangled regions of Hilbert space. The purpose of this paper is to examine the phase ( $\gamma$ )-dependence of the entanglement and the applicable domains for the most general qubit-interchange-symmetric three-qubit states. First, we compute the eigenvalues of the non-linear eigenvalue equations and the nearest separable states for the permutation-invariant three-qubit states with a fixed phase. Next, we compute the geometric entanglement measure, find allocations of highly- and slightly-entangled states and deduce the boundaries of all subspaces. Given a fixed  $\gamma$ , the boundary is the set of states for which eigenvalues of the stationarity equations are degenerate. Thus, the boundary separates subspaces with different eigenvalues, and these eigenvalues coincide on the boundary. When  $\gamma \neq \pi/2$ , there are two invariant subspaces, and boundary states are double degenerate. The entanglement of quantum states is phase independent in the first subspace and increases with  $\gamma$  in the second subspace. However, there are three invariant subspaces at  $\gamma = \pi/2$ , and boundary states are either doubly or triply (among them infinitely) degenerate.

PACS numbers: 03.67.Mn, 03.65.Ud

Keywords: Geometric measure of entanglement

DOI: 10.3938/jkps.58.1058

### I. INTRODUCTION

Entanglement is a property of quantum states that does not exist classically. Two or more subsystems of a quantum system are said to be entangled if the state of the entire system cannot be described in terms of a state for each of the subsystems [1]. This property of composite quantum systems, which exhibits quantum correlations between subsystems, is a resource for many processes in quantum information theory [2–5]. Since the profound measures of entanglement, *i.e.*, the entanglement of formation and distillation [6–9], have not been properly generalized to multiparticle systems, the study of quantifying multipartite entanglement via other measures [10–14] is a necessity.

The entanglement of a given pure state can be characterized by the distance to the nearest unentangled state [15]. A whole class of such entanglement monotones, based on the Euclidean distance of a given multipartite state to the nearest fully separable state, was constructed in Ref. 16. Subsequently, a geometrically motivated measure of entanglement, known as the geometric measure, was introduced by Wei and Goldbart [17]. It is a de-

creasing function of the maximal overlap  $P_{max}$  and is suitable for any partite system regardless of its dimensions. The maximal overlap has several different names, and we list all of them for the completeness: maximal probability of success [13], entanglement eigenvalue [17], injective tensor norm [18], the largest Schmidt coefficient [19] and maximum singular value [20].

The geometric measure has an advantage in that it can be computed analytically for multi-parameter states. Recently, explicit expressions for the maximal overlap have been derived for three- [17,20–23], as well as for multi-qubit states [24–27]. It turned out that the maximal overlap, depending on the coefficients of a quantum state in a computational basis, can be interpreted in two different ways. It is equal to either the square of the largest coefficient or the square of the circumradius of a cyclic polygon constructed by using the coefficients of the quantum state. However, there are states for which both formulae are true, and the largest coefficients coincides with that of circumradius. Consequently, these states, known as shared quantum states [22], have two different nearest product states that result in the same maximal overlap. An example is the GHZ state  $(|000\rangle + |111\rangle)/\sqrt{2}$ , where  $|000\rangle$  and  $|111\rangle$  are two such “degenerate” product states with  $P_{max} = 1/2$ . The maximal overlap is the maximum

\*E-mail: dkpark@kyungnam.ac.kr

singular value [20] of a given state; thus, the maximum singular value of shared states is degenerate. Obviously, this degeneracy is independent of the choice of the state parameters (as well as of the choice of the computational basis), and shared states form a parametrization invariant set. On the other hand, shared states separate two types of states, namely, those for which the maximal overlap is the largest coefficient and those for which the maximal overlap is the circumradius of a cyclic polygon. This means that the whole parameter space is divided into two subspaces, each of which has its own expression for the geometric measure.

In spite of these achievements, still we lack sufficient knowledge to classify generic three-qubit pure states by using the geometric measure. They have five local unitary (LU) invariants, including four positive parameters and a gauge phase  $\gamma$  [19,28,29]. The maximal overlap of these states is not known yet. Only three-qubit states, which are expressed as linear combinations of four (or less) orthogonal product states, have been considered so far [22]. In fact, all of these states have real coefficients because the phases of their coefficients can be eliminated by LU-transformations. Thus, the contribution of the gauge phase to the maximal overlap remains a mystery. On the other hand, the most recent results [30] have shown that the gauge phase plays an important role. It parameterizes the family of maximally entangled states and identifies W-class pure states with the boundary of pure states.

In this paper, we would like to take into account the effect of the gauge phase in the geometric measure of entanglement. We compute the maximal overlap, as well as the nearest product states, for a given value of the gauge phase. We will show in the following that, depending on the phase factor  $\gamma$ , the whole parameter space is divided into two or three domains, each of which has a particular expression for the geometric measure. In addition, we will show that most highly entangled states reside near the boundaries of the domains. This is a direct consequence of the fact that for all the maximally entangled states, the maximum singular value should be degenerate [30]; therefore, the maximally entangled states are a subset of the shared states that form the boundaries. Thus, highly entangled states are located around the maximally entangled states as one would expect. We will call these highly entangled states as GHZ neighbors because each of them can be transformed to the GHZ state via stochastic local operations and classical communications. The states located far from the boundaries become less-entangled and eventually go to the product states, but there is a different kind of the highly entangled states. These states reside around W states and can be converted to the W-state by invertible local operations. We will call these highly entangled states as W neighbors. The W neighbors are generally more entangled than the GHZ neighbors from the aspect of the geometric measure. However, the range of the GHZ neighbors is much wider than the range of the W neigh-

bors.

The paper is organized as follows: In Section II, following Ref. 21, we transform the nonlinear eigenvalue equations into the Lagrange multiplier equations. In Section III, we solve the Lagrange multiplier equations analytically for  $\gamma = 0$  and  $\gamma = \pi/2$ . It turns out that both cases give five different eigenvalues. Also, every eigenvalue has its own available region in the parameter space. In Section IV, we compute the geometric measure for the  $\gamma = 0$  case. It turns out that two of the five eigenvalues contribute to the geometric measure. This means that the whole parameter space is divided into two applicable domains. In Section V, we compute the geometric measure for the  $\gamma = \pi/2$  case. We show that the whole parameter space is divided into three applicable domains. In Section VI, we compute the eigenvalues and the geometric measure for  $\gamma = \pi/4$  numerically. We show that when  $\gamma = \pi/4$ , there are six different eigenvalues. However, only two eigenvalues contribute to the geometric measure. In Section VII, based on the numerical calculation, we examine the  $\gamma$ -dependence of the geometric entanglement measure and the characteristics of the applicable domains. We show that there are states that stay in one applicable domain over the full range of the phase. The remaining states move from one to another domain by passing the boundary when the phase increases. We also show that the phase factor either enhances or leaves unchanged, but never decreases, the entanglement. In Section VIII, a brief conclusion is given. In the appendix, we have shown that the Lagrange multiplier equations for arbitrary  $\gamma$  provide a solution whose multiplier constant is zero.

## II. GENERAL FORMALISM

In this section, we clarify our notations, give necessary definitions, define three-qubit symmetric states and transform nonlinear stationarity equations to a system of linear equations.

### 1. Preliminaries

The maximal overlap of a given  $n$ -qubit pure state  $|\psi\rangle$  is given by

$$P_{\max} = \max_{q_1, q_2, \dots, q_n} |(\langle q_1 | \otimes \langle q_2 | \otimes \cdots \otimes \langle q_n |) |\psi\rangle|^2, \quad (1)$$

where the maximization is performed over single-qubit pure states. Constituents  $|q_1\rangle, |q_2\rangle, \dots, |q_n\rangle$ , the nearest product state from  $|\psi\rangle$ , can be computed via the nonlinear eigenvalue equations

$$\begin{aligned} \langle q_1 | \cdots \langle q_{n-1} | \psi \rangle &= \mu_i |q_n\rangle, \quad \langle q_1 | \cdots \\ \langle q_{n-2} | \langle q_n | \psi \rangle &= \mu_i |q_{n-1}\rangle, \quad \cdots, \\ \langle q_2 | \cdots \langle q_n | \psi \rangle &= \mu_i |q_1\rangle, \end{aligned} \quad (2)$$

where  $\mu_i$ 's are the eigenvalues of Eq. (2). Then, the geometric measure  $G$  of the quantum state  $|\psi\rangle$  is defined as  $G(\psi) = 1 - P_{max}$ , where  $P_{max} = \max(\mu_i^2)$ .

Any pure three-qubit state can be written as a superposition of five product states as follows [19,28,30]:

$$|\psi\rangle = g|000\rangle + t_1|011\rangle + t_2|101\rangle + t_3|110\rangle + e^{i\gamma}h|111\rangle, \quad (3)$$

where the labels within each ket refer to qubits A, B, and C (or 1, 2, and 3) in that order and in what follows we will continue to identify qubits only by the ordering of the labels. The coefficients of the decomposition in Eq. (3) should be positive, and the phase should vary within the interval  $[-\pi/2, \pi/2]$ ; that is

$$g, t_1, t_2, t_3, h \geq 0, -\frac{\pi}{2} \leq \gamma \leq \frac{\pi}{2}. \quad (4)$$

The generalized Schmidt decomposition in Eq. (3) is based on the geometric measure of entanglement and is the best parametrization for our investigation. It can be derived as follows. Consider any solution of the stationarity equations in Eq. (2) for a given state  $|\psi\rangle$  and denote it by  $|q_1q_2q_3\rangle$ . For each single-qubit state  $|q_k\rangle$  ( $k = 1, 2, 3$ ), there is, up to arbitrary phase, a unique single-qubit state  $|p_k\rangle$  orthogonal to it. From these single-qubit states  $|q_k\rangle$  and  $|p_k\rangle$ , one can form a set of 8 three-qubit product states, which form a basis in Hilbert space. Now, the state  $|\psi\rangle$  can be written as a linear combination of these product states and, owing to stationarity equations, the coefficients of the product states  $|q_1q_2p_3\rangle$ ,  $|q_1p_2q_3\rangle$ , and  $|p_1q_2q_3\rangle$  should vanish. One can also relabel the closest product  $|q_1q_2q_3\rangle$  as  $|000\rangle$  and, then, adjust the phases of the local states  $|0_k\rangle$  and  $|1_k\rangle$  so that the inequalities in Eq. (4) are satisfied.

The generalized Schmidt decomposition in Eq. (3) distinguishes all five types of inequivalent entanglements of pure three-qubits [31]. Consider the first three types of bi-separable states, namely, states bi-separable with respect to the partitions A:BC, B:AC, and C:AB. The state is bi-separable if and only if (see the brief proof in Ref. 30)

$$gh^2 = 0 \quad \text{and} \quad t_1t_2t_3 = 0. \quad (5)$$

Moreover, the state is separable with respect to the A:BC bipartition, that is, qubit A is unentangled, if either  $g = t_1 = 0$  or  $h = t_2 = t_3 = 0$ . Similarly, the qubit B(C) is unentangled if  $g = t_2 = 0$  or  $h = t_1 = t_3 = 0$  ( $g = t_3 = 0$  or  $h = t_1 = t_2 = 0$ ).

The state is a W-class state if and only if

$$\begin{aligned} \text{either } g &= 0 \text{ and } t_1t_2t_3 \neq 0, \\ \text{or } gh^2 &= 4t_1t_2t_3 \neq 0 \text{ and } \gamma = \pm\pi/2. \end{aligned} \quad (6)$$

All the remaining states are GHZ-class states. In conclusion, the coefficients of the generalized Schmidt decomposition in Eq. (3) are physically meaningful and classify clearly pure three-qubit states.

For simplicity, we take quantum states that possess permutational symmetry [32–34]. These states have three independent parameters and, through an appropriate LU transformations, can be brought into the symmetric form

$$|\psi\rangle = g|000\rangle + t|011\rangle + t|101\rangle + t|110\rangle + e^{i\gamma}h|111\rangle, \quad (7)$$

where we follow the notation of Ref. 30. We would like to apply the general method proposed in Ref. 21 to the symmetric states in Eq. (7). Since the maximal overlap is an even function in  $\gamma$ , in what follows we will consider only positive values of the phase.

## 2. Modified Stationarity Equations

In this subsection, we would like to present the method for solving stationarity equations for the quantum state given in Eq. (7). In the case of three-qubit pure states, the method developed in Ref. 21 transforms the system of nonlinear equations to a system of linear equations. In spite of this essential simplification, it is impossible to get analytic expressions for generic three-qubit states because the solution to the linear eigenvalue equations reduces to the finding the roots for a couple of algebraic equations of degree six [22]. However, the permutation symmetry of  $|\psi\rangle$  reduces this pair of algebraic equations to a single algebraic equation of degree six. Furthermore, there is a solution, which holds for all values of the state parameters [30]. The separation of this global solution allows us to solve explicitly the eigenvalue equations for  $\gamma = 0$  and  $\gamma = \pi/2$  and leads us to a quartic equation for the remaining cases. The quartic is the highest-order polynomial equation that can be solved by radicals in the general case. However, expressions for roots are impractical, so we will carry out numerical analysis instead.

The method enables us to express the eigenvalues  $\mu^2$  via the reduced densities  $\rho^A$ ,  $\rho^B$ , and  $\rho^{AB}$  of qubits A and B in the form

$$\mu^2 = \frac{1}{4} \max_{|\mathbf{s}_1|=|\mathbf{s}_2|=1} (1 + \mathbf{r}_1 \cdot \mathbf{s}_1 + \mathbf{r}_2 \cdot \mathbf{s}_2 + G_{ij}s_{1i}s_{2j}), \quad (8)$$

where

$$\begin{aligned} \mathbf{r}_1 &= \text{Tr}(\rho^A \boldsymbol{\sigma}), & \mathbf{r}_2 &= \text{Tr}(\rho^B \boldsymbol{\sigma}), \\ G_{ij} &= \text{Tr}(\rho^{AB} \sigma_i \otimes \sigma_j) \end{aligned} \quad (9)$$

and  $\sigma_i$ 's are Pauli matrices. An explicit calculation shows

$$\begin{aligned} \mathbf{r} &\equiv \mathbf{r}_1 = \mathbf{r}_2 = (2ht \cos \gamma, 2ht \sin \gamma, g^2 - h^2 - t^2) \\ G_{ij} &= \begin{pmatrix} 2t(g+t) & 0 & -2ht \cos \gamma \\ 0 & -2t(g-t) & -2ht \sin \gamma \\ -2ht \cos \gamma & -2ht \sin \gamma & g^2 + h^2 - t^2 \end{pmatrix}. \end{aligned} \quad (10)$$

It is worthwhile noting that  $\mathbf{r}_1$  is identical with  $\mathbf{r}_2$  and that  $G_{ij}$  is a symmetric matrix. These properties arise

due to the fact that we have chosen the symmetric state in Eq. (7) under the qubit exchange. As will be shown in the following, these properties drastically simplify the calculation procedure. Since  $\mathbf{r}_1$ ,  $\mathbf{r}_2$ , and  $G_{ij}$  are explicitly derived, the eigenvalues  $\mu^2$  can be computed if  $\mathbf{s}_1$  and  $\mathbf{s}_2$  are known. Due to the maximization in Eq. (8), these vectors can be computed by solving the Lagrange multiplier equations:

$$\mathbf{r}_1 + G\mathbf{s}_2 = \lambda_1 \mathbf{s}_1, \quad \mathbf{r}_2 + G^T \mathbf{s}_1 = \lambda_2 \mathbf{s}_2, \quad (11)$$

where the superscript  $T$  stands for transpose and the  $\lambda_i$ 's are the Lagrange multiplier constants. From the properties  $\mathbf{r}_1 = \mathbf{r}_2$  and  $G_{ij} = G_{ji}$ , Eq. (11) can be reduced to a single equation

$$\mathbf{r} + G\mathbf{s} = \lambda \mathbf{s}, \quad (12)$$

where  $\lambda \equiv \lambda_1 = \lambda_2$  and  $\mathbf{s} \equiv \mathbf{s}_1 = \mathbf{s}_2$ . Letting

$$\mathbf{s} = (\sin \theta \cos \varphi, \sin \theta \sin \varphi, \cos \theta), \quad (13)$$

Eq. (12) reduces to

$$2ht \cos \gamma + 2t(g+t) \sin \theta \cos \varphi - 2ht \cos \gamma \cos \theta = \lambda \sin \theta \cos \varphi, \quad (14a)$$

$$2ht \sin \gamma - 2t(g-t) \sin \theta \sin \varphi - 2ht \sin \gamma \cos \theta = \lambda \sin \theta \sin \varphi, \quad (14b)$$

$$(g^2 - t^2)(1 + \cos \theta) - h^2(1 - \cos \theta) - 2ht \cos \gamma \sin \theta \cos \varphi - 2ht \sin \gamma \sin \theta \sin \varphi = \lambda \cos \theta. \quad (14c)$$

Solving for  $\theta$ ,  $\varphi$ , and  $\lambda$  from Eq. (14), one can compute the eigenvalues for the symmetric canonical state in Eq. (7) by inserting the solutions into Eq. (8). In the next section, we will solve analytically Eq. (14) at the particular phases  $\gamma = 0$  and  $\gamma = \pi/2$ . By making use of the solutions, we will compute  $\mu_i$  and  $P_{max} = \max(\mu_i^2)$  for the corresponding quantum states.

### III. EIGENVALUES

In this section, Eq. (14) will be solved at  $\gamma = 0$  and  $\pi/2$  separately. Since a numerical calculation is needed to analyze the  $\gamma = \pi/4$  case, we deal with this case in a different section (see section VI).

#### 1. $\gamma = 0$ Case

For the  $\gamma = 0$  case, Eq. (14) reduces to

$$2t(g+t) \sin \theta \cos \varphi + 2ht(1 - \cos \theta) = \lambda \sin \theta \cos \varphi, \quad (15a)$$

$$-2t(g-t) \sin \theta \sin \varphi = \lambda \sin \theta \sin \varphi, \quad (15b)$$

$$(g^2 - t^2)(1 + \cos \theta) - h^2(1 - \cos \theta) - 2ht \sin \theta \cos \varphi = \lambda \cos \theta. \quad (15c)$$

Equation (15b) implies that the solutions for the  $\gamma = 0$  case are categorized by  $\theta = 0$ ,  $\varphi = 0$ ,  $\varphi = \pi$ , and  $\lambda = -2t(g-t)$ <sup>1</sup>. For the  $\theta = 0$  case, Eq. (15a) and Eq. (15b) are automatically solved, and Eq. (15c) gives

$$\lambda = 2(g^2 - t^2). \quad (16)$$

Now,  $\mathbf{s} = (0, 0, 1)$  and Eq. (8), together with the normalization condition  $g^2 + 3t^2 + h^2 = 1$ , give a eigenvalue

$$\mu_P^2 = g^2. \quad (17)$$

For the  $\varphi = 0$  case, Eq. (15) is automatically solved, and the remaining equations are

$$2t(g+t) \sin \theta + 2ht(1 - \cos \theta) = \lambda \sin \theta, \quad (18a)$$

$$(g^2 - t^2)(1 + \cos \theta) - h^2(1 - \cos \theta) - 2ht \sin \theta = \lambda \cos \theta. \quad (18b)$$

Since  $\sin(\theta/2) \neq 0$ , Eq. (18a) reduces to

$$\lambda = 2htz + 2t^2 + 2tg, \quad (19)$$

where  $z = \tan(\theta/2)$ . Inserting Eq. (19) into Eq. (18b), one can derive

$$(hz + g + t)(tz^2 - hz + g - 2t) = 0, \quad (20)$$

which implies that the  $\varphi = 0$  case is categorized by the following three cases:

$$z = -\frac{g+t}{h}, \quad \frac{r_+}{2t}, \quad \frac{r_-}{2t}, \quad (21)$$

where

$$r_{\pm} = h \pm \sqrt{h^2 + 4t(2t-g)}. \quad (22)$$

First, let us consider the case of  $z = -(g+t)/h$ . In this case, Eq. (19) gives

$$\lambda = 0. \quad (23)$$

Since, in this case,

$$\begin{aligned} s_x &= \sin \theta = -\frac{2h(g+t)}{h^2 + (g+t)^2}, & s_y &= 0, \\ s_z &= \frac{h^2 - (g+t)^2}{h^2 + (g+t)^2}, \end{aligned} \quad (24)$$

it is straightforward to compute the eigenvalues for this case, which is

$$\mu_1^2 = \frac{g^2h^2 + t^2(g+t)^2}{h^2 + (g+t)^2}. \quad (25)$$

<sup>1</sup> The case  $\theta = \pi$  can be excluded by Eq. (15a) unless  $ht = 0$ . If  $t = 0$ ,  $|\psi\rangle$  reduces to the usual GHZ state whose  $P_{max}$  is  $\max(g^2, h^2)$ . If  $h = 0$ , the maximal overlap probability for  $|\psi\rangle$  is fully discussed in Ref. 22.

Table 1. Eigenvalues for the  $\gamma = 0$  case.

name	eigenvalue	$\lambda$	available region
$\mu_P^2$	$\frac{g^2}{h^2 + (g+t)^2}$	$2(g^2 - t^2)$	all
$\mu_1^2$	$\frac{g^2 h^2 + t^2(g+t)^2}{h^2 + (g+t)^2}$	0	all
$\mu_+^2$	$\frac{(hr_+ + 4t^2)^2}{r_+^2 + 4t^2}$	$hr_+ + 2t(g+t)$	$g \leq 2t + h^2/(4t)$
$\mu_-^2$	$\frac{(hr_- + 4t^2)^2}{r_-^2 + 4t^2}$	$hr_- + 2t(g+t)$	$g \leq 2t + h^2/(4t)$
$\mu_2^2$	$\frac{g(gh^2 + 4t^3)}{g^2 + h^2 + 3gt}$	$2t(t-g)$	$(3g - 2t)h^2 + 4g^2t \geq 0$

Next, let us consider the cases of  $z = r_{\pm}/2t$  simultaneously. In these cases, Eq. (19) gives

$$\lambda = hr_{\pm} + 2t(g+t). \quad (26)$$

Since, in these cases,

$$s_x = \frac{4tr_{\pm}}{r_{\pm}^2 + 4t^2}, \quad s_y = 0, \quad s_z = -\frac{r_{\pm}^2 - 4t^2}{r_{\pm}^2 + 4t^2}, \quad (27)$$

one can show directly that the eigenvalues are

$$\mu_{\pm}^2 = \frac{(hr_{\pm} + 4t^2)^2}{r_{\pm}^2 + 4t^2}. \quad (28)$$

Since  $z = \tan(\theta/2)$  should be real, the eigenvalues  $\mu_{\pm}^2$  are available only when

$$g \leq 2t + \frac{h^2}{4t}. \quad (29)$$

For the  $\varphi = \pi$  case Eq. (15) is automatically solved, and the remaining equations are

$$-2t(g+t)\sin\theta + 2ht(1-\cos\theta) = -\lambda\sin\theta, \quad (30a)$$

$$(g^2 - t^2)(1 + \cos\theta) - h^2(1 - \cos\theta) + 2ht\sin\theta = \lambda\cos\theta. \quad (30b)$$

Since Eq. (30) can be derived from Eq. (18) by changing  $\theta \rightarrow -\theta$ , the solutions for this case are also categorized by

$$z = \frac{g+t}{h}, \quad -\frac{r_+}{2t}, \quad -\frac{r_-}{2t}. \quad (31)$$

Since Eq. (30a) reduces to

$$\lambda = -2htz + 2t^2 + 2tg, \quad (32)$$

comparison of Eq. (32) with Eq. (19) shows that the Lagrange multiplier constant  $\lambda$  is the same as that for the case of  $\varphi = 0$ . Since, furthermore,  $s_x = \sin\theta\cos\varphi$  and  $s_z = \cos\theta$  are invariant under  $\theta \rightarrow -\theta$  and  $\varphi = 0 \rightarrow \varphi = \pi$ , the eigenvalues for this case are exactly the same as those for the  $\varphi = 0$  case.

For the  $\lambda = 2t^2 - 2gt$  case, Eq. (15) is automatically solved, and the remaining equations are

$$2t(g+t)\sin\theta\cos\varphi + 2ht(1 - \cos\theta) = -2t(g-t)\sin\theta\cos\varphi, \quad (33a)$$

$$(g^2 - t^2)(1 + \cos\theta) - h^2(1 - \cos\theta) - 2ht\sin\theta\cos\varphi = -2t(g-t)\cos\theta. \quad (33b)$$

Since Eq. (33a) gives a relation

$$\cos\varphi = -\frac{h}{2g} \frac{1 - \cos\theta}{\sin\theta}, \quad (34)$$

combining Eq. (33b) and Eq. (34) enables us to express  $\cos\theta$  and  $\sin\theta$  as

$$\begin{aligned} \cos\theta &= -\frac{g^2 - h^2 + gt}{g^2 + h^2 + 3gt}, \\ \sin\theta &= \pm \frac{\sqrt{4g(g+2t)(h^2+gt)}}{g^2 + h^2 + 3gt}. \end{aligned} \quad (35)$$

For the time being, we choose the upper sign in  $\sin\theta$ . Then, Eq. (34) reduces to

$$\cos\varphi = \frac{h}{2} \sqrt{\frac{g+2t}{g(h^2+gt)}}. \quad (36)$$

At this stage, it is worthwhile noting that the eigenvalue in this case is available when

$$(3g - 2t)h^2 + 4g^2t \geq 0 \quad (37)$$

because  $-1 \leq \cos\varphi \leq 1$ . Of course, the corresponding  $\sin\varphi$  is

$$\sin\varphi = \pm \sqrt{\frac{3gh^2 + 4g^2t - 2h^2t}{4g(h^2+gt)}}. \quad (38)$$

Again, we choose the upper sign in  $\sin\varphi$ . Then, it is straightforward to compute  $s$ , whose components are

$$\begin{aligned} s_x &= -\frac{h(g+2t)}{g^2 + h^2 + 3gt}, \\ s_y &= \frac{\sqrt{(g+2t)(3gh^2 + 4g^2t - 2h^2t)}}{g^2 + h^2 + 3gt}, \\ s_z &= -\frac{g^2 - h^2 + gt}{g^2 + h^2 + 3gt}. \end{aligned} \quad (39)$$

Inserting Eq. (39) into Eq. (8) gives the eigenvalue for this case as follow:

$$\mu_2^2 = \frac{g(gh^2 + 4t^3)}{g^2 + h^2 + 3gt}. \quad (40)$$

It is easy to show that the choice of the other sign in  $\sin\theta$  and  $\sin\varphi$  does not change the eigenvalue  $\mu_2^2$ . The eigenvalues for the  $\gamma = 0$  case are summarized in Table 1.

## 2. $\gamma = \pi/2$ Case

For the  $\gamma = \pi/2$  case, Eq. (14) reduces to

$$2t(g+t)\sin\theta\cos\varphi = \lambda\sin\theta\cos\varphi, \quad (41a)$$

$$\begin{aligned} -2t(g-t)\sin\theta\sin\varphi + 2ht(1-\cos\theta) \\ = \lambda\sin\theta\sin\varphi, \end{aligned} \quad (41b)$$

$$\begin{aligned} (g^2 - t^2)(1 + \cos\theta) - h^2(1 - \cos\theta) \\ - 2ht\sin\theta\sin\varphi = \lambda\cos\theta. \end{aligned} \quad (41c)$$

Equation (41a) guarantees that the solutions for this case are categorized by  $\theta = 0$ ,  $\varphi = \pi/2$ ,  $\varphi = 3\pi/2$ , and  $\lambda = 2t(g+t)$ . Since the calculation procedure for the first three cases are similar to those for the  $\gamma = 0$  case, we will briefly sketch the final result only. Although the calculation procedure for the last case is also similar to therefor the previous case, it gives a non-trivial available region, which is important for computing the geometric measures in the next section. Therefore, we will present the last case in detail.

When  $\theta = 0$ , the Lagrangian multiplier constant is the same as for Eq. (16), and the corresponding eigenvalue is

$$\nu_P^2 = g^2. \quad (42)$$

When  $\varphi = \pi/2$ , there are three types of solutions, depending on  $z = \tan(\theta/2)$ . If  $z = (g-t)/h$ , we have a vanishing Lagrange multiplier constant, and the corresponding eigenvalue is

$$\nu_1^2 = \frac{g^2h^2 + t^2(g-t)^2}{h^2 + (g-t)^2}. \quad (43)$$

When  $z = s_{\pm}/2t$ , where

$$s_{\pm} = h \pm \sqrt{h^2 + 4t(2t+g)}, \quad (44)$$

the corresponding Lagrange multiplier constants are  $hs_{\pm} - 2t(g-t)$ , and the corresponding eigenvalues are

$$\nu_{\pm}^2 = \frac{(hs_{\pm} + 4t^2)^2}{s_{\pm}^2 + 4t^2}. \quad (45)$$

It should be noted that  $\nu_{\pm}^2$  are available in the entire parameter space while  $\mu_{\pm}^2$  in the  $\gamma = 0$  case is restricted by Eq. (29). As in the case of  $\gamma = 0$ , the  $\varphi = 3\pi/2$  case

does not give a new eigenvalue. This case just reproduces  $\nu_1^2$  and  $\nu_{\pm}^2$ .

Finally, let us discuss the  $\lambda = 2t(g+t)$  case. For this case, Eq. (41a) is automatically solved, and the remaining equations are

$$\begin{aligned} 2ht(1 - \cos\theta) - 2t(g - t)\sin\theta\sin\varphi \\ = 2t(g + t)\sin\theta\sin\varphi, \end{aligned} \quad (46a)$$

$$\begin{aligned} (g^2 - t^2)(1 + \cos\theta) - h^2(1 - \cos\theta) - 2ht\sin\theta\sin\varphi \\ = 2t(g + t)\cos\theta. \end{aligned} \quad (46b)$$

Since Eq. (46a) gives a relation

$$\sin\varphi = \frac{h}{2g} \frac{1 - \cos\theta}{\sin\theta}, \quad (47)$$

combining Eq. (46b) and Eq. (47) yields

$$\cos\theta = -\frac{g^2 - h^2 - gt}{g^2 + h^2 - 3gt}. \quad (48)$$

The requirement  $-1 \leq \cos\theta \leq 1$  gives the first available condition

$$(g - 2t)(h^2 - gt) \geq 0. \quad (49)$$

Now, we choose  $\sin\theta$  as

$$\sin\theta = \frac{\sqrt{4g(g-2t)(h^2-gt)}}{g^2 + h^2 - 3gt}. \quad (50)$$

Then, from Eq. (47)  $\sin\varphi$  becomes

$$\sin\varphi = \frac{h}{2} \sqrt{\frac{g-2t}{g(h^2-gt)}}. \quad (51)$$

Another requirement,  $-1 \leq \sin\varphi \leq 1$ , gives the second available condition:

$$(g - 2t)(3gh^2 - 4g^2t + 2h^2t) \geq 0. \quad (52)$$

Choosing  $\cos\varphi$  as

$$\cos\varphi = \sqrt{\frac{3gh^2 - 4g^2t + 2h^2t}{4g(h^2 - gt)}}, \quad (53)$$

it is straightforward to show that the eigenvalues for this case is

$$\nu_2^2 = \frac{g(gh^2 - 4t^3)}{g^2 + h^2 - 3gt}. \quad (54)$$

It is easy to show that the different choices in the sign of  $\sin\theta$  and/or  $\cos\varphi$  do not change the eigenvalue. Although the available region for  $\nu_2^2$  is restricted by Eq. (49) and Eq. (52), one can show that Eq. (52) implies Eq. (49) already. To show this explicitly, let us consider the  $g \geq 2t$  case first. In this case, Eq. (52) imposes  $h^2 \geq 4g^2t/(3g+2t)$ . Therefore,

$$h^2 - gt \geq \frac{4g^2t}{3g+2t} - gt = \frac{gt}{3g+2t}(g-2t) \geq 0.$$

Similarly, one can show that Eq. (52) implies Eq. (49) for the  $g \leq 2t$  region, too. Therefore, the available region for  $\nu_2^2$  is restricted by Eq. (52) only. The eigenvalues in the  $\gamma = \pi/2$  case is summarized in Table 2.

Table 2. Eigenvalues for the  $\gamma = \pi/2$  case.

name	eigenvalue	$\lambda$	available region
$\nu_P^2$	$g^2$	$2(g^2 - t^2)$	all
$\nu_1^2$	$\frac{g^2 h^2 + t^2(g-t)^2}{h^2 + (g-t)^2}$	0	all
$\nu_+^2$	$\frac{(hs_+ + 4t^2)^2}{s_+^2 + 4t^2}$	$hs_+ - 2t(g-t)$	all
$\nu_-^2$	$\frac{(hs_- + 4t^2)^2}{s_-^2 + 4t^2}$	$hs_- - 2t(g-t)$	all
$\nu_2^2$	$\frac{g(gh^2 - 4t^3)}{g^2 + h^2 - 3gt}$	$2t(g+t)$	$(g-2t)(3gh^2 - 4g^2t + 2h^2t) \geq 0$

### 3. $h \rightarrow 0$ Limit

Since  $|\psi\rangle$  is independent of  $\gamma$  in the  $h \rightarrow 0$  limit, all eigenvalues for  $\gamma = 0$  and  $\gamma = \pi/2$  should be the same, including the available region in the parameter space. Note that  $\mu_+^2 = \mu_-^2$  and  $\nu_+^2 = \nu_-^2$  in the  $h \rightarrow 0$  limit. In this limit, the eigenvalues for  $\gamma = 0$  exactly coincide with the eigenvalues for  $\gamma = \pi/2$ :

$$\begin{aligned} \mu_P^2 &= \nu_P^2 = g^2, & \mu_1^2 &= \nu_1^2 = t^2, \\ \mu_{\pm}^2 &= \nu_{\pm}^2 = \frac{4t^3}{3t+g}, & \mu_{\pm}^2 &= \nu_{\pm}^2 = \frac{4t^3}{3t-g}. \end{aligned} \quad (55)$$

In addition, the first three eigenvalues in Eq. (55) are available in the full parameter space, and the last one is available only at  $g \leq 2t$ . Thus, our calculational results are perfectly consistent in the  $h \rightarrow 0$  limit.

### IV. GEOMETRIC MEASURE FOR $\gamma = 0$

In this section, we would like to compute the geometric entanglement measure defined by

$$G(\psi) = 1 - P_{max}(\psi) \quad (56)$$

for the  $\gamma = 0$  case. In order to compute  $P_{max}$ , we would like to emphasize three points, which simplify the following calculation. Firstly, note that  $P_{max}$  is given by

$$P_{max} = \max(\mu_i^2). \quad (57)$$

Therefore, we should choose the largest eigenvalue from all eigenvalues, each of which has its own available region in the parameter space. Secondly, note that

$$\mu_+^2 - \mu_-^2 = \frac{128ht^{7/2}}{(r_+^2 + 4t^2)(r_-^2 + 4t^2)} \left( 2t + \frac{h^2}{4t} - g \right)^{3/2}. \quad (58)$$

This means that  $\mu_-^2$  is always smaller than  $\mu_+^2$  in the available region  $g \leq 2t + h^2/(4t)$ . Therefore, we can exclude  $\mu_-^2$  from beginning for the computation of  $P_{max}$ . Thirdly, note that  $P_{max}$  is obtained from the eigenvalues

whose Lagrange multiplier constants are positive [21]. This fact excludes  $\mu_1^2$ , too. Considering all of these facts and the available regions, it is convenient to divide the whole parameter space into the following four regions:

$$\begin{aligned} \text{(region I)} \quad g &\geq 2t + \frac{h^2}{4t} : & P_{max} &= \mu_P^2 \\ \text{(region II)} \quad t &\leq g \leq 2t + \frac{h^2}{4t} : & P_{max} &= \max(\mu_P^2, \mu_+^2) \\ \text{(region III)} \quad g &\leq t \ \& \mathcal{C}_1 \geq 0 : & P_{max} &= \max(\mu_+^2, \mu_2^2) \\ \text{(region IV)} \quad g &\leq t \ \& \mathcal{C}_1 \leq 0 : & P_{max} &= \mu_+^2, \end{aligned} \quad (59)$$

where

$$\mathcal{C}_1 = (3g - 2t)h^2 + 4g^2t. \quad (60)$$

In order to compare  $\mu_+^2$  with  $\mu_2^2$ , we compute  $\mu_+^2 - \mu_2^2$ , which is

$$\begin{aligned} \mu_+^2 - \mu_2^2 &= \frac{2}{(r_+^2 + 4t^2)(g^2 + h^2 + 3gt)} \\ &\times \left( \alpha_1 + \beta_1 \sqrt{h^2 + 4t(2t-g)} \right), \end{aligned} \quad (61)$$

where

$$\begin{aligned} \alpha_1 &= h^6 + gh^4t + 8h^4t^2 + 20gh^2t^3 + 16g^2t^4 \\ &\quad + 4h^2t^2(2t^2 - g^2), \\ \beta_1 &= h(h^4 + 3gh^2t + 4g^2t^2 + 4h^2t^2 + 8gt^3). \end{aligned} \quad (62)$$

Since the last term in  $\alpha_1$ ,  $4h^2t^2(2t^2 - g^2)$  is non-negative in the region  $g \leq t$ , both  $\alpha_1$  and  $\beta_1$  are non-negative in region III. In region III, therefore,  $P_{max}$  becomes  $\mu_+^2$ .

In region II it has been shown in Ref. 30 that  $\mu_P^2 = \mu_+^2$  when  $\mathcal{D}_1 = 0$ , where

$$\mathcal{D}_1 = gh^2 - (g+t)^2(g-2t). \quad (63)$$

Therefore, region II should be divided into two regions, i.e.,  $\mathcal{D}_1 \geq 0$  and  $\mathcal{D}_1 \leq 0$ . Simple consideration shows that  $\mu_P^2 \geq \mu_+^2$  when  $\mathcal{D}_1 \leq 0$  and  $\mu_P^2 \leq \mu_+^2$  when  $\mathcal{D}_1 \geq 0$ . Combining all of these facts, one can conclude that

$$\text{(region A)} \quad g \geq 2t + \frac{h^2}{4t} : \quad P_{max} = \mu_P^2 \quad (64)$$

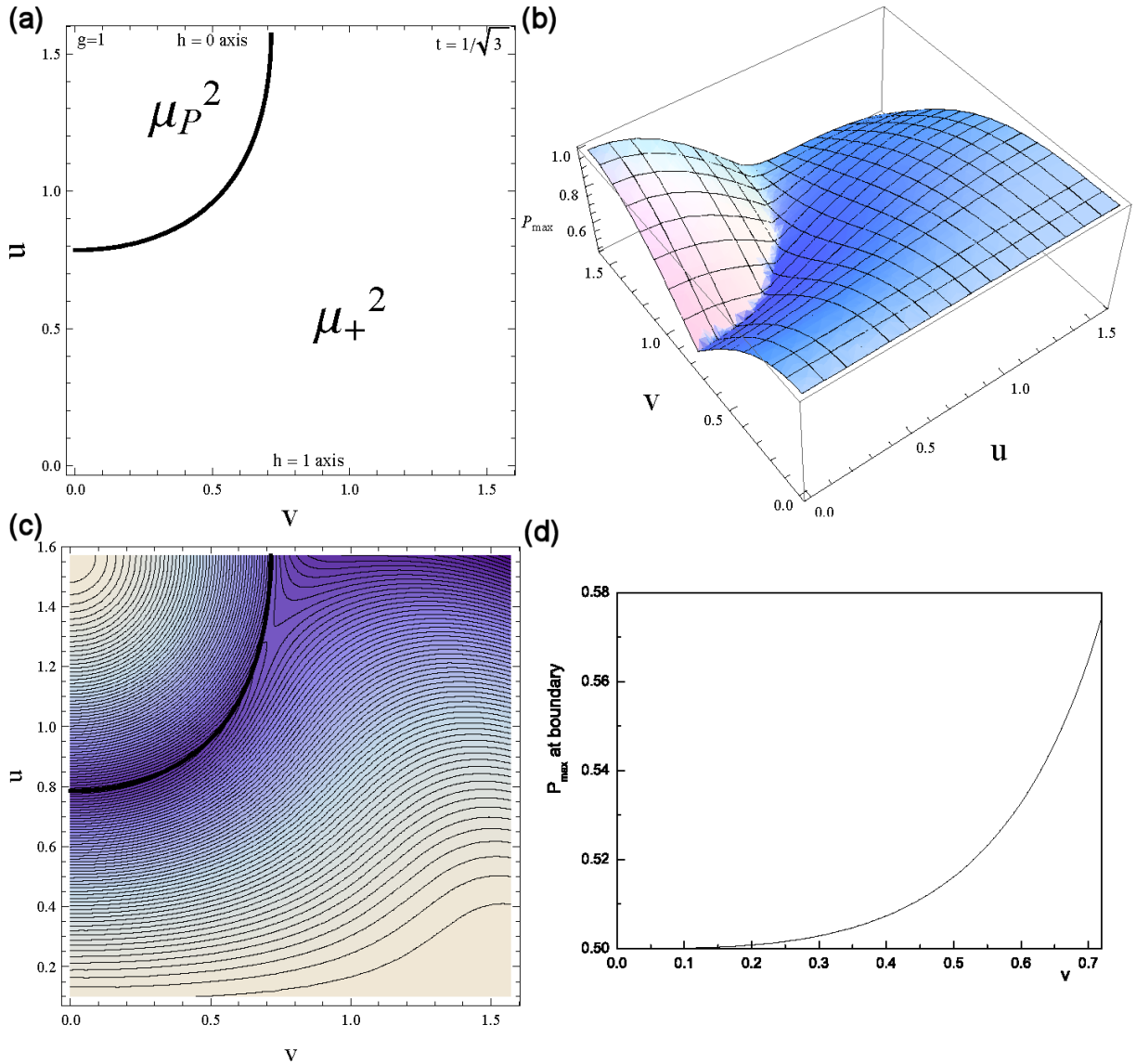


Fig. 1. (Color online) (a) Plot of the applicable domains in the  $(u, v)$ -plane for  $\gamma = 0$ . The principal domain  $P_{\max} = \mu_P^2$  is located in the small- $v$ , large- $u$  region. This fact indicates that this domain is around the large- $g$  region. (b) Plot of the  $(u, v)$  dependence of  $P_{\max}$  for the  $\gamma = 0$  case. Many highly entangled states are represented as a valley in this figure. Around  $u \sim 0$  and  $(u \sim \pi/2, v \sim 0)$ , there are many less entangled states. To compare the applicable domains with  $P_{\max}$ , we plot both simultaneously in the  $(u, v)$  plane in (c). The black thick line is the boundary between domains. The blue color and the white color represent the highly- and less-entangled states, respectively. (c) shows that the highly-entangled states reside around the boundary between domains. (d) shows the  $v$ -dependence of  $P_{\max}$  for the shared states, *i.e.*, for states located at the boundary.

$$\begin{aligned}
 \text{(region B)} \quad & t \leq g \leq 2t + \frac{h^2}{4t} \quad \& \quad \mathcal{D}_1 \leq 0 : \quad P_{\max} = \mu_P^2 \\
 \text{(region C)} \quad & t \leq g \leq 2t + \frac{h^2}{4t} \quad \& \quad \mathcal{D}_1 \geq 0 : \quad P_{\max} = \mu_+^2 \\
 \text{(region D)} \quad & g \leq t : \quad P_{\max} = \mu_+^2.
 \end{aligned}$$

Now, we would like to unify the regions as much as possible to simplify the expression of  $P_{\max}$ . First, one can show that  $\mathcal{D}_1$  is always non-positive in region A as follows: Since  $h^2 \leq 4t(g - 2t)$  in region A, in this region,

$$\mathcal{D}_1 = gh^2 - (g+t)^2(g-2t) \leq -(g-2t)(g-t)^2 \leq 0. \quad (65)$$

Second, one can show easily that  $\mathcal{D}_1$  is always non-negative in region D as follows: In this region,

$$\mathcal{D}_1 = gh^2 + (g+t)^2(2t-g) \geq 0 \quad (66)$$

because both terms are non-negative. Combining these facts and Eq. (64),  $P_{\max}$  can be expressed as

$$P_{\max} = \begin{cases} \mu_P^2 & \text{when } \mathcal{D}_1 \leq 0 \\ \mu_+^2 & \text{when } \mathcal{D}_1 \geq 0. \end{cases} \quad (67)$$

Consider now states with  $D_1 = 0$  (designated as shared quantum states in Ref. 22). For these states, both eigen-

values  $\mu_P^2$  and  $\mu_+^2$  coincide, so the maximal eigenvalue of the nonlinear equations, Eq. (2), is doubly degenerate. For a pure state of three qubits, it is possible to write different generalized Schmidt decompositions by using only five elements of the whole Hilbert space basis. Each decomposition has its own entanglement parameters that are LU-invariant quantities. Regardless of the choice of the generalized Schmidt decomposition (and state parameters), the maximal eigenvalue of Eq. (2) is either degenerate or not. Therefore, the set of shared quantum states does not depend on a particular parametrization of three-qubit states and presents a special class of states in Hilbert space. The same is true for the two classes of states given by  $D_1 < 0$  and  $D_1 > 0$ . Indeed, one cannot transform a state from  $D_1 < 0$  to  $D_1 > 0$  (and vice-versa) by re-parameterizations or LU-transformations because in order to do so, one has to pass the surface  $D_1 = 0$ , meaning that one is able to change the degeneracy of eigenvalues of stationarity equations, Eq. (2). Thus, the Hilbert space is divided into two subspaces, namely,  $D_1 < 0$  and  $D_1 > 0$ , and these subspaces are separated by shared states  $D_1 = 0$ . Shared states can be ascribed to both subspaces and, owing to this, may acquire new features [21].

In order to understand the behavior of  $P_{max}$  more clearly, we introduce the two parameters  $u$  and  $v$  as follows:

$$g = \sin u \cos v, \quad t = \sin u \sin v / \sqrt{3}, \quad h = \cos u, \quad (68)$$

with  $0 \leq u, v \leq \pi/2$ . Then, one can plot the applicable domains  $D_1 \leq 0$  and  $D_1 \geq 0$  in the  $u - v$  plane, which is Fig. 1(a). As Fig. 1(a) shows, the domain for  $D_1 \leq 0$  is biased in the small- $v$ , large- $u$  region. This indicates that the domain for  $D_1 \leq 0$  are around the large- $g$  region. The remaining region is the domain for  $D_1 \geq 0$ . As will be shown in the next section, the number of the applicable domains for the  $\gamma = \pi/2$  case is not two, but three. This means that the phase factor  $\gamma$  has a great impact on the geometric measure of entanglement.

Figure 1(b) shows the  $(u, v)$  dependence of  $P_{max}$  given in Eq. (67). At  $u = 0$ , which means  $h = 1$ ,  $P_{max}$  becomes 1 because it is a separable state. At  $v = 0$  and  $u = \pi/2$ , which means that  $g = 1$ ,  $P_{max}$  becomes 1 again. Between them, there is valley, which represents the set of highly entangled states. There is a different kind of highly entangled states around  $u = v = \pi/2$ . These highly entangled states are states located near a W state,  $|W\rangle = (1/\sqrt{3})(|011\rangle + |101\rangle + |110\rangle)$ .

In order to compare  $P_{max}$  with the applicable domains, we plot  $P_{max}$  and the boundary of domains simultaneously in the  $u - v$  plane in Fig. 1(c). In Fig. 1(c), the black thick line is a boundary of the domains. The thick blue and the light-blue (or white) colors represent the highly-entangled and the less-entangled states, respectively. In the right-upper corner, there are many highly-entangled states, which are located near the W state. Another type of highly entangled state resides near the boundary of the applicable domains. Apart from the boundary more and

more, quantum states lose entanglement and eventually reduce to separable states.

Since the shared states, *i.e.*, states located at the boundary of the applicable domain, may have special features for quantum information processing [21,22], we would like to compute  $P_{max}$  for the shared states located at  $D_1 = 0$ . The condition  $D_1 = 0$  makes it possible to express  $u$  in terms of  $v$ . Therefore,  $P_{max}$  at the boundary can be easily expressed in terms of  $v$  only as

$$P_{max} = \frac{\cos^3 v}{\cos v + \left(\cos v + \frac{1}{\sqrt{3}} \sin v\right)^2 \left(\cos v - \frac{2}{\sqrt{3}} \sin v\right)}. \quad (69)$$

The  $v$ -dependence of  $P_{max}$  in Eq. (69) is plotted in Fig. 1(d). Figure 1(d) shows that  $P_{max}$  increases monotonically with increasing  $v$  from  $1/2$  (at  $v = 0$ ) to  $4/7$  (at  $v = \tan^{-1} \sqrt{3}/2$ ).

Now, we consider several special cases. The first example is  $t = 1/\sqrt{3}$  and  $g = h = 0$ . In this case,  $D_1 = 2\sqrt{3}/9 > 0$ , and  $r_+ = \sqrt{8/3}$ , which gives  $P_{max} = 4/9$ . The second example is  $t = 0$  and  $g \geq h$ . In this case,  $D_1 = -g(g^2 - h^2) \leq 0$ , and  $P_{max} = g^2$ . The third example is  $t = 0$  and  $g \leq h$ . In this case,  $D_1 = g(h^2 - g^2) \geq 0$ , and  $r_+ = 2h$ , which gives  $P_{max} = h^2$ . The second and the third examples are consistent with  $P_{max}(GHZ) = \max(|\alpha|^2, |\beta|^2)$ , where  $|GHZ\rangle = \alpha|000\rangle + \beta|111\rangle$ . The fourth example is the  $g = 0$  case. In this case,  $D_1 = 2t^3 \geq 0$ , and  $r_+ = h + \sqrt{h^2 + 8t^2}$ , which results in

$$P_{max} = \frac{(h^4 + 8h^2t^2 + 8t^4) + h(h^2 + 4t^2)\sqrt{h^2 + 8t^2}}{(h^2 + 6t^2) + h\sqrt{h^2 + 8t^2}}. \quad (70)$$

One can show that various limits of Eq. (70) are consistent with previously-derived results. The last example is the  $h = 0$  case. In this case, it is easy to show that

$$P_{max} = \begin{cases} g^2, & \text{when } g \geq 2t \\ 4t^3/(3t - g), & \text{when } g \leq 2t. \end{cases} \quad (71)$$

Equation (71) is perfectly in agreement with the result of Ref. 22.

## V. GEOMETRIC MEASURE FOR $\gamma = \pi/2$

In this section, we would like to compute the geometric entanglement measure for the  $\gamma = \pi/2$  case. From the constraint of the positive Lagrange multiplier constant, we can exclude  $\nu_1^2$  and  $\nu_-^2$  from the beginning stage for the computation of the geometric measure. Next, we should examine the sign of the Lagrange multiplier constant for  $\nu_+^2$ , that is,

$$\lambda_+ = hs_+ - 2t(g - t). \quad (72)$$

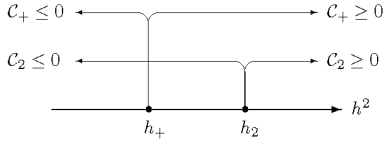


Fig. 2. Pictorial representation for  $C_2 \geq 0$ ,  $C_2 \leq 0$ ,  $C_+ \geq 0$ , and  $C_+ \leq 0$  when  $g \geq t$ .

It is easy to show that  $\lambda_+ \geq 0$  in the  $g \leq t$  region. Also, it is straightforward to show that  $\lambda_+ \geq 0$  when  $C_+ \geq 0$  and that  $\lambda_+ \leq 0$  when  $C_+ \leq 0$ , where

$$C_+ = h^2(2g + t) - t(g - t)^2. \quad (73)$$

Examining Table 2 and Eq. (73) lead us to divide the whole parameter space into the following ten regions:

$$(i) \quad g \geq 2t \quad (74)$$

$$\text{(region I)} \quad C_2 \leq 0 \text{ & } C_+ \leq 0 : \quad P_{max} = \nu_P^2$$

$$\text{(region II)} \quad C_2 \geq 0 \text{ & } C_+ \leq 0 :$$

$$P_{max} = \max(\nu_P^2, \nu_2^2) \quad (75)$$

$$\text{(region III)} \quad C_2 \leq 0 \text{ & } C_+ \geq 0 :$$

$$P_{max} = \max(\nu_P^2, \nu_+^2) \quad (76)$$

$$\text{(region IV)} \quad C_2 \geq 0 \text{ & } C_+ \geq 0 :$$

$$P_{max} = \max(\nu_P^2, \nu_+^2, \nu_2^2) \quad (77)$$

$$(ii) \quad t \leq g \leq 2t$$

$$\text{(region V)} \quad C_2 \geq 0 \text{ & } C_+ \leq 0 :$$

$$P_{max} = \nu_P^2 \quad (78)$$

$$\text{(region VI)} \quad C_2 \leq 0 \text{ & } C_+ \leq 0 :$$

$$P_{max} = \max(\nu_P^2, \nu_2^2) \quad (79)$$

$$\text{(region VII)} \quad C_2 \geq 0 \text{ & } C_+ \geq 0 :$$

$$P_{max} = \max(\nu_P^2, \nu_+^2) \quad (80)$$

$$\text{(region VIII)} \quad C_2 \leq 0 \text{ & } C_+ \geq 0 :$$

$$P_{max} = \max(\nu_P^2, \nu_+^2, \nu_2^2) \quad (81)$$

$$(iii) \quad g \leq t$$

$$\text{(region IX)} \quad C_2 \leq 0 : P_{max} = \max(\nu_+^2, \nu_2^2)$$

$$\text{(region X)} \quad C_2 \geq 0 : P_{max} = \nu_+^2,$$

where

$$C_2 = (3g + 2t)h^2 - 4g^2t. \quad (82)$$

Although the whole space is divided into ten regions, one can show that some regions do not exist. In order to show this, it is convenient to introduce

$$h_2 = \frac{4g^2t}{3g + 2t}, \quad h_+ = \frac{t(g - t)^2}{2g + t}. \quad (83)$$

Then, their difference becomes

$$h_2 - h_+ = \frac{t(g + t)^2}{(3g + 2t)(2g + t)}(5g - 2t). \quad (84)$$

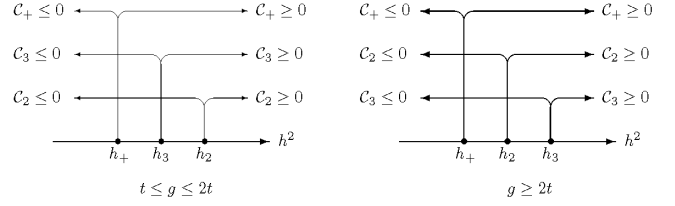


Fig. 3. Pictorial representations for  $C_2 \geq 0$ ,  $C_2 \leq 0$ ,  $C_+ \geq 0$ ,  $C_+ \leq 0$ ,  $C_3 \geq 0$ , and  $C_3 \leq 0$  when (a)  $t \leq g \leq 2t$  and (b)  $g \geq 2t$ .

Equation (84) implies that  $h_2 \geq h_+$  in the region  $g \geq t$ . Then, the regions  $C_2 \geq 0$ ,  $C_2 \leq 0$ ,  $C_+ \geq 0$ , and  $C_+ \leq 0$  when  $g \geq t$  can be represented as in Fig. 2. With the help of Fig. 2, it is easy to understand that there is no region that satisfies both  $C_2 \geq 0$  and  $C_+ \leq 0$  when  $g \geq t$ . This implies that region II and region V do not exist in the whole parameter space.

In order to compare  $\nu_P^2$  with  $\nu_2^2$ , we compute  $\nu_P^2 - \nu_2^2$ , which is

$$\nu_P^2 - \nu_2^2 = \frac{g(g + t)(g - 2t)^2}{g^2 + h^2 - 3gt}. \quad (85)$$

Therefore, the sign of  $\nu_P^2 - \nu_2^2$  is determined by  $g^2 + h^2 - 3gt$ . If  $C_2 \geq 0$ ,  $h^2 \geq h_2$  and

$$g^2 + h^2 - 3gt \geq \frac{3g(g - 2t)(g + t)}{3g + 2t}. \quad (86)$$

Therefore, if  $C_2 \geq 0$  in the  $g \geq 2t$  region,  $\nu_P^2 \geq \nu_2^2$ . Thus, we can exclude  $\nu_2^2$  in region IV. Similarly, one can show that if  $C_2 \leq 0$  in the  $t \leq g \leq 2t$  region,  $\nu_P^2 \leq \nu_2^2$ . Therefore, we can exclude  $\nu_P^2$  in regions VI and VIII.

Next, we compute  $\nu_P^2 - \nu_+^2$ , which is

$$\nu_P^2 - \nu_+^2 = \frac{2}{s_+^2 + 4t^2} \left( \alpha_2 + \beta_2 \sqrt{h^2 + 4t(2t + g)} \right), \quad (87)$$

where

$$\begin{aligned} \alpha_2 &= -h^4 + (g + 2t)(g - 4t)h^2 + 2t(g - t)(g + 2t)^2, \\ \beta_2 &= h(g^2 - h^2 - 4t^2). \end{aligned} \quad (88)$$

A direct calculation shows that in the  $g \geq t$  region,  $\nu_P^2 = \nu_+^2$  when  $C_3 = 0$ , where

$$C_3 = gh^2 - (g - t)^2(g + 2t). \quad (89)$$

In addition, a simple consideration shows that in the  $g \geq t$  region,  $\nu_P^2 \geq \nu_+^2$  when  $C_3 \leq 0$ , and  $\nu_P^2 \leq \nu_+^2$  when  $C_3 \geq 0$ .

In order to check which eigenvalue is dominant in each region, it is convenient to introduce another parameter

$$h_3 = \frac{(g - t)^2(g + 2t)}{g}. \quad (90)$$

Then, it is easy to show that

$$h_+ \leq h_2 \leq h_3 \quad \text{when } 2t \leq g, \quad (91)$$

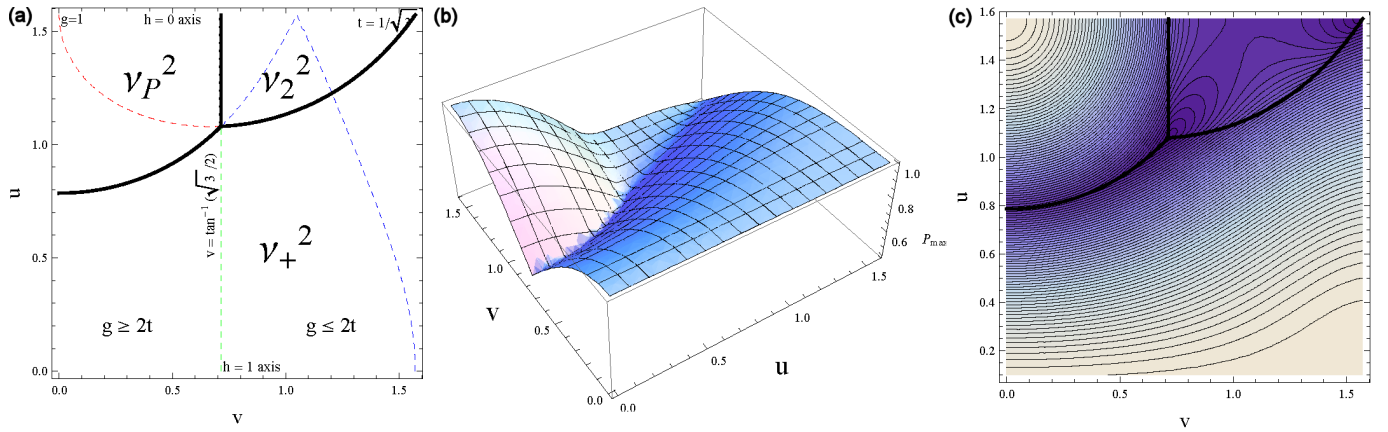


Fig. 4. (Color online) (a) Plot of the applicable domains for the  $\gamma = \pi/2$  case in the  $(u, v)$ -plane. Unlike the  $\gamma = 0$  case there are three applicable domains in this case. The principal domain  $P_{max} = \nu_P^2$  is larger than  $P_{max} = \mu_P^2$  in the  $\gamma = 0$  case. This fact seems to indicate that the principal domain increases its territory with increasing  $\gamma$ . It is important to note that the domain  $P_{max} = \nu_+^2$  does not reach the  $h = 0$  axis. This implies the consistency of the  $h \rightarrow 0$  limit. (b)  $(u, v)$  dependence of  $P_{max}$ . The highly entangled states forms a valley between two mountains. (c) Plot of  $P_{max}$  and the applicable domains in the  $(u, v)$ -plane. The boundaries of the domains are represented by thick black lines. Many highly entangled states reside around the boundaries and in the domain  $P_{max} = \nu_+^2$ . This is mainly due to the fact that there are two LU-equivalent W states for the  $\gamma = \pi/2$  case.

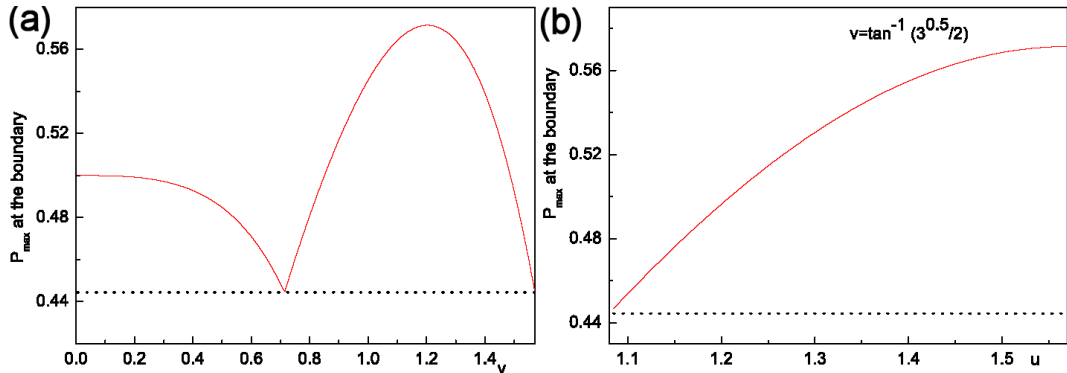


Fig. 5. (Color online)  $P_{max}$  at the boundaries of the applicable domains when  $\gamma = \pi/2$ . (a) shows the  $v$ -dependence of  $P_{max}$  for  $C_3 = 0$  (boundary between  $\nu_P^2$  and  $\nu_+^2$ ) and  $C_2 = 0$  (boundary between  $\nu_+^2$  and  $\nu_2^2$ ). (b) shows the  $u$ -dependence of  $P_{max}$  for the boundary between  $\nu_P^2$  and  $\nu_2^2$ . The dotted line denotes  $4/9$ , which is  $P_{max}$  of the W state.

$$h_+ \leq h_3 \leq h_2 \quad \text{when } t \leq g \leq 2t.$$

Equation (91) enables us to represent  $C_2 \geq 0$ ,  $C_2 \leq 0$ ,  $C_+ \geq 0$ ,  $C_+ \leq 0$ ,  $C_3 \geq 0$ , and  $C_3 \leq 0$  in a one-dimensional coordinate, which is illustrated in Fig. 3. With the help of Fig. 3, one can show easily that in region III,  $C_3$  is always non-positive; therefore,  $P_{max}$  becomes  $\nu_P^2$ . Using Fig. 3(a),  $P_{max}$  in region VII is  $\nu_+^2$ . Using Fig. 3(b), again one can show that region IV is divided into

- (region IV-a)  $C_2 \geq 0 \text{ \& } C_3 \leq 0 : \quad P_{max} = \nu_P^2 \quad (92)$   
 (region IV-b)  $C_2 \geq 0 \text{ \& } C_3 \geq 0 : \quad P_{max} = \nu_+^2.$

Finally, we compute  $\nu_+^2 - \nu_2^2$ , which is

$$\begin{aligned} \nu_+^2 - \nu_2^2 &= \frac{2}{(s_+^2 + 4t^2)(g^2 + h^2 - 3gt)} \\ &\times \left( \alpha_3 + \beta_3 \sqrt{h^2 + 4t(2t + g)} \right), \end{aligned} \quad (93)$$

where

$$\begin{aligned} \alpha_3 &= h^6 + t(8t - g)h^4 \\ &\quad - 4t^2(g^2 + 5gt - 2t^2)h^2 + 16g^2t^4, \\ \beta_3 &= h [h^4 + t(4t - 3g)h^2 + 4gt^2(g - 2t)]. \end{aligned} \quad (94)$$

One can show directly that  $\nu_+^2 - \nu_2^2 = 0$  when  $C_2 = 0$ . Also, it is straightforward to show that in the  $g \leq 2t$  region,  $\nu_+^2$  is always smaller than  $\nu_2^2$ . Therefore, we can exclude  $\nu_+^2$  in regions VIII and IX. Combining all of these facts, one can express  $P_{max}$  for the  $\gamma = \pi/2$  case as follows:

$$\begin{cases} \nu_+^2 & \text{if } \mathcal{C}_2 \geq 0 \text{ \& } \mathcal{C}_3 \geq 0 \\ \nu_P^2 & \text{remaining region} \\ \nu_+^2 & \text{(i) } g \geq 2t \\ \nu_P^2 & \text{(ii) } g \leq 2t \end{cases}$$

$$P_{max} = \begin{cases} \nu_+^2 & \mathcal{C}_2 \geq 0 \\ \nu_2^2 & \mathcal{C}_2 \leq 0. \end{cases} \quad (95)$$

Unlike the  $\gamma = 0$  case, the whole parameter space is divided into the three applicable domains. Now we have three types of shared states:

- doubly degenerate states  $\nu_+^2 = \nu_P^2 \neq \nu_2^2$ ,
- doubly degenerate states  $\nu_+^2 = \nu_2^2 \neq \nu_P^2$ ,
- triply (some of them infinitely [30]) degenerate states  $\nu_+^2 = \nu_2^2 = \nu_P^2$ .

Introducing the parameters  $u$  and  $v$  as Eq. (68), we plot the three applicable domains in the  $u$ - $v$  plane in Fig. 4(a). Around the  $h = 0$  axis, there are two domains, *i.e.*,  $\nu_P^2$  and  $\nu_2^2$ . Since  $\nu_P^2$  and  $\nu_2^2$  go to  $\mu_P^2$  and  $\mu_+^2$  in the  $h \rightarrow 0$  limit, this guarantees that the  $h \rightarrow 0$  limit is consistent with the same limit as in the  $\gamma = 0$  case. The applicable domain for  $\nu_P^2$  is a little bit larger than the domain  $\mu_P^2$  for the  $\gamma = 0$  case. The point ( $u = \cos^{-1}(\sqrt{2}/3)$ ,  $v = \tan^{-1}(\sqrt{3}/2)$ ) is shared by three domains. This point corresponds to

$$\begin{aligned} |\psi_W\rangle = & \frac{2}{3}|000\rangle + \frac{1}{3}(|011\rangle + |101\rangle + |110\rangle) \\ & + i\frac{\sqrt{2}}{3}|111\rangle. \end{aligned} \quad (96)$$

This is LU-equivalent with  $|W\rangle = (1/\sqrt{3})(|100\rangle + |010\rangle + |001\rangle)$ , as shown in Ref. 30.

In Fig. 4(b), we plot the  $(u, v)$  dependence of  $P_{max}$  given in Eq. (95). Like Fig. 1(b) the highly entangled

states are represented as a valley in this figure. Figure 4(b) seems to show that there exists an alley in the valley, which ends at  $u = v = \pi/2$ . Along this alley, so many highly entangled states are located. Comparing Fig. 4(b) with Fig. 1(b), one can realize that there are many more highly-entangled states for the  $\gamma = \pi/2$  case than the  $\gamma = 0$  case. This is mainly due to the fact that there are two LU-equivalent W states when  $\gamma = \pi/2$ .

Figure 4(c) shows the geometric entanglement measure and the applicable domains simultaneously in the  $u$ - $v$  plane. Figure 4(c) shows that around two W states there are so many highly entangled states, which we would like to call W neighbors. Especially, the neighbors of  $|\psi_W\rangle$  in Eq. (96) gather along the  $\mathcal{C}_3 = 0$  line. Besides the W neighbors, there are many highly entangled states around the boundary of the applicable domains. These are the neighbors of the shared states [22], and we would like to call them the GHZ neighbors. The GHZ neighbors are slightly less-entangled compared to the W neighbors. However, the number of the GHZ neighbors is much larger than that of the W neighbors.

The maximal overlap probability  $P_{max}$  at the boundaries can be computed as follows: The boundary conditions  $\mathcal{C}_2 = 0$  (between  $\nu_2^2$  and  $\nu_+^2$ ) and  $\mathcal{C}_3 = 0$  (between  $\nu_P^2$  and  $\nu_+^2$ ) make it possible to express  $u$  in terms of  $v$ . Then, it is straightforward, but a slightly tedious, to express  $P_{max}$  in terms of  $v$  only as follows:

$$P_{max} = \begin{cases} f_1(v) & 0 \leq v \leq \tan^{-1}(\sqrt{3}/2) \\ f_2(v) & \tan^{-1}(\sqrt{3}/2) \leq v \leq \pi/2, \end{cases} \quad (97)$$

where

$$\begin{aligned} f_1(v) &= \frac{\cos^3 v}{\cos v + \left(\cos v - \frac{1}{\sqrt{3}}\sin v\right)^2 \left(\cos v + \frac{2}{\sqrt{3}}\sin v\right)}, \\ f_2(v) &= \frac{4\sin v(3\sqrt{3}\cos v + 2\sin v)[9\cos^3 v - \sqrt{3}\sin^2 v(3\sqrt{3}\cos v + 2\sin v)]}{9(3\sqrt{3}\cos v + 2\sin v + 4\sin v\cos^2 v)(3\cos v + \sqrt{3}\sin v)(\sqrt{3}\cos v - 2\sin v)}. \end{aligned} \quad (98)$$

The  $v$ -dependence of  $P_{max}$  is plotted in Fig. 5(a). In the region  $0 \leq v \leq \tan^{-1}(\sqrt{3}/2)$ , which is a boundary between  $\nu_P^2$  and  $\nu_2^2$ ,  $P_{max}$  decreases from  $1/2$  to  $4/9$ . These two values correspond to the usual GHZ and  $|\psi_W\rangle$  states. In the region  $\tan^{-1}(\sqrt{3}/2) \leq v \leq \pi/2$ , which is a boundary between  $\nu_2^2$  and  $\nu_+^2$ ,  $P_{max}$  increases from  $4/9$  to  $0.57$  and decreases to  $4/9$  again, which corresponds to the usual W state  $(1/\sqrt{3})(|100\rangle + |010\rangle + |001\rangle)$ . At the boundary between  $\nu_P^2$  and  $\nu_2^2$ ,  $v$  is fixed by  $v = \tan^{-1}(\sqrt{3}/2)$ . Then,  $P_{max}$  can be easily expressed in terms of  $u$  only in the form

$$P_{max} = \frac{4}{7}\sin^2 u, \quad (\cos^{-1}\sqrt{2}/3 \leq u \leq \pi/2). \quad (99)$$

This is plotted in Fig. 5(b), which shows that  $P_{max}$  increases monotonically with increasing  $u$  from  $4/9$  to its maximal value 0.571.

Finally, we consider several special cases. The first example is the  $h = 0$  case. In this case,  $\mathcal{C}_2 = -4g^2t \leq 0$  and  $\mathcal{C}_3 = -(g-t)^2(g+2t) \leq 0$ , which results an expression identical to that of Eq. (71). Therefore, results for both the  $\gamma = 0$  and the  $\gamma = \pi/2$  cases coincide with each other in the  $h \rightarrow 0$  limit. The second example is the  $t = 0$  case. It is easy to show that in this case,  $P_{max} = g^2$  when  $g \geq h$  and that  $P_{max} = h^2$  when  $g \leq h$ . This is consistent with  $P_{max}(\text{GHZ}) = \max(|\alpha|^2, |\beta|^2)$  when  $|\text{GHZ}\rangle = \alpha|000\rangle + \beta|111\rangle$ .

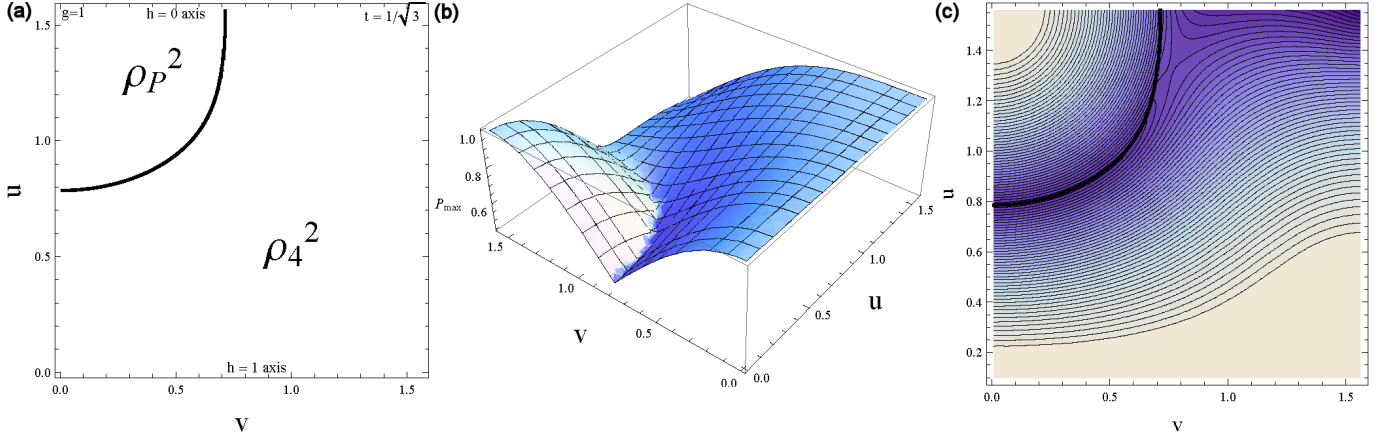


Fig. 6. (Color online) (a) Plot of the applicable domains for the  $\gamma = \pi/4$  case. In this case, there are two applicable domains. The principal domain  $P_{max} = \rho_P^2$ , is little bit larger than the  $P_{max} = \mu_P^2$  domain for  $\gamma = 0$  and little bit smaller than the  $P_{max} = \nu_P^2$  domain for  $\gamma = \pi/2$ . This fact indicates that the principal domain increases its territory with increasing  $\gamma$ . (b)  $(u, v)$  dependence of  $P_{max}$ . As in the  $\gamma = 0$  case, the highly entangled states form a valley between two mountains. (c) Plot of  $P_{max}$  and the applicable domains in the  $(u, v)$ -plane. Many highly entangled states reside around the boundary of the domains and near the W state.

## VI. EIGENVALUES AND GEOMETRIC MEASURE FOR $\gamma = \pi/4$ : NUMERICAL APPROACH

In this section, we will compute the eigenvalues and the geometric measure for the  $\gamma = \pi/4$  case.

### 1. Eigenvalues

For  $\gamma = \pi/4$ , Eq. (14) reduces to

$$2t(g+t)\sin\theta\cos\varphi + \sqrt{2}ht(1-\cos\theta) = \lambda\sin\theta\cos\varphi, \quad (100a)$$

$$-2t(g-t)\sin\theta\sin\varphi + \sqrt{2}ht(1-\cos\theta) = \lambda\sin\theta\sin\varphi, \quad (100b)$$

$$(g^2 - t^2)(1 + \cos\theta) - h^2(1 - \cos\theta) - \sqrt{2}ht\sin\theta(\sin\varphi + \cos\varphi) = \lambda\cos\theta. \quad (100c)$$

When  $\theta = 0$ , Eq. (100a) and Eq. (100b) are automatically solved, and Eq. (100c) gives

$$\lambda = 2(g^2 - t^2). \quad (101)$$

Since  $s = (0, 0, 1)$  for this case, from Eq. (8), the corresponding eigenvalue is

$$\rho_P^2 = g^2. \quad (102)$$

When  $\sin\theta \neq 0$ , Eq. (100a) and Eq. (100b) reduce to

$$z = \frac{\lambda - 2gt - 2t^2}{\sqrt{2}ht} \cos\varphi = \frac{\lambda + 2gt - 2t^2}{\sqrt{2}ht} \sin\varphi, \quad (103)$$

where  $z = \tan(\theta/2)$ . From Eq. (103), one can compute  $\varphi$ , if  $\lambda$  is known, by using

$$\tan\varphi = \frac{(\lambda - 2t^2) - 2gt}{(\lambda - 2t^2) + 2gt}. \quad (104)$$

Deriving  $\sin\varphi + \cos\varphi$  from Eq. (103) and inserting it into Eq. (100c), one can derive the expression for  $z^2$  in the form

$$z^2 = \frac{[(\lambda - 2t^2)^2 - 4g^2t^2](\lambda - 2g^2 + 2t^2)}{(\lambda - 2h^2)(\lambda - 2t^2)^2 - 8h^2t^2(\lambda - 2t^2) - 4g^2t^2(\lambda - 2h^2)}. \quad (105)$$

On the other hand, one can derive a different expression for  $z^2$  directly from Eq. (103):

$$z^2 = \frac{(\lambda - 2gt - 2t^2)^2}{2h^2t^2}(1 + \tan^2\varphi)^{-1}$$

$$= \frac{[(\lambda - 2t^2)^2 - 4g^2t^2]^2}{4h^2t^2[(\lambda - 2t^2)^2 + 4g^2t^2]}. \quad (106)$$

Equating Eq. (105) with Eq. (106) yields an equation for solely  $\lambda$ :

$$\lambda f(\lambda) = 0, \quad (107)$$

where

$$\begin{aligned} f(\lambda) = & \lambda^4 - 2(h^2 + 4t^2)\lambda^3 - 4t^2(2g^2 - h^2 - 6t^2)\lambda^2 \\ & + 8[t^4(h^2 - 4t^2) + g^2(3h^2t^2 + 4t^4)]\lambda \\ & + 16t^4(g^4 - 5g^2h^2 - 2g^2t^2 - h^2t^2 + t^4). \end{aligned} \quad (108)$$

Equation (107) guarantees the existence of an eigenvalue for  $\lambda = 0$  as in the  $\gamma = 0$  and  $\gamma = \pi/2$  cases. In fact, one can show that there exists an eigenvalue corresponding to  $\lambda = 0$  for arbitrary  $\gamma$ . We have shown this fact in Appendix A.

When  $\lambda = 0$ , Eq. (104) and Eq. (106) reduce to

$$z^2 = \frac{(g^2 - t^2)^2}{h^2(g^2 + t^2)}, \quad \tan \varphi = -\frac{g+t}{g-t}. \quad (109)$$

Combining Eq. (103) and Eq. (109), the possible solutions for  $\theta$  and  $\varphi$  are

$$\begin{aligned} z &= \pm \frac{g^2 - t^2}{h\sqrt{g^2 + t^2}}, \quad \cos \varphi = \mp \frac{g-t}{\sqrt{2(g^2 + t^2)}}, \\ \sin \varphi &= \pm \frac{g+t}{\sqrt{2(g^2 + t^2)}}. \end{aligned} \quad (110)$$

It is easy to show that both solutions in Eq. (110) give the same eigenvalue, which is

$$\rho_0^2 = \frac{g^2(g^2 + t^2)h^2 + t^2(g^2 - t^2)^2}{h^2(g^2 + t^2) + (g^2 - t^2)^2}. \quad (111)$$

Finally, let us consider  $f(\lambda) = 0$ . It is worthwhile noting that in the  $h \rightarrow 0$  limit,  $f(\lambda) = 0$  reduces to  $(\lambda - 2gt - 2t^2)^2(\lambda + 2gt - 2t^2)^2 = 0$ . Therefore, the eigenvalues corresponding to  $f(\lambda) = 0$  should coincide with  $\mu_{\pm}^2$  and  $\mu_0^2$  for the  $\gamma = 0$  case, and with  $\nu_{\pm}^2$  and  $\nu_0^2$  for the  $\gamma = \pi/2$  case in the  $h \rightarrow 0$  limit. Equation  $f(\lambda) = 0$  gives four solutions for  $\lambda$ , say  $\lambda_1, \lambda_2, \lambda_3$ , and  $\lambda_4$ . We ordered the solutions by using the fact that the  $h \rightarrow 0$  limit of  $\lambda_1$  and  $\lambda_2$  is  $-2t(g-t)$  and that the same limit of  $\lambda_3$  and  $\lambda_4$  is  $2t(g+t)$ . Then, the corresponding eigenvalues, say  $\rho_1^2, \rho_2^2, \rho_3^2$ , and  $\rho_4^2$ , can be computed numerically.

## 2. Geometric Measure

Using eigenvalues  $\rho_P^2, \rho_0^2$  derived analytically and  $\rho_i^2$  ( $i = 1, 2, 3, 4$ ) computed numerically, one can compute  $P_{max}$  for the  $\gamma = \pi/4$  case. Since each eigenvalue has its own available region, we checked this region by imposing  $\text{Re}[\lambda] = 0, -1 \leq \sin \theta \leq 1, -1 \leq \cos \theta \leq 1, -1 \leq \sin \varphi \leq 1$ , and  $-1 \leq \cos \varphi \leq 1$ . Although there are six different eigenvalues, the numerical calculation

shows that only  $\rho_P^2$  and  $\rho_4^2$  contribute to the geometric measure. This indicates that the whole parameter space is divided into two applicable domains. These two domains are represented in the  $u - v$  plane in Fig. 6(a). The domains  $\rho_P^2$  is slightly larger than domain  $\mu_P^2$  and slightly smaller than the domain  $\nu_P^2$ . This fact seems to indicate that the domain containing  $g = 1$  extends its territory with increasing  $\gamma$ .

Figure 6(b) shows the  $(u, v)$  dependence of  $P_{max}$  for  $\gamma = \pi/4$ . Similar to the  $\gamma = 0$  and the  $\pi/2$  cases, many highly entangled states reside at the valley between two mountains. Another highly entangled state resides around  $u = v = \pi/2$ , which corresponds to a W state. The alley that appears in Fig. 4(b) does not appear in this case. This seems to be due to the fact that there is only one W state in the  $\gamma = \pi/4$  case.

Figure 6(c) shows the  $(u, v)$  dependence of  $P_{max}$  and its domains. As expected, the highly entangled states are located around the boundary and the W state.

## VII. THE $\gamma$ -DEPENDENCE OF THE MAXIMAL OVERLAP

In this section, we would like to describe the  $\gamma$ -dependence of  $P_{max}$  and the applicable domains. The results described in this section are based on numerical calculations. However, in order to gain a better insight into the numerical results, we start from a preliminary analytic description.

The solutions to Eq. (14) are degenerate if the three equations linearly depend on the value of the Lagrange multiplier given by Eq. (16)<sup>2</sup>. This means that  $\det(G - \lambda_0 \mathbb{1}) = 0$ , which has the following explicit form:

$$(g^2 - t^2)^2(g^2 - 4t^2) = gh^2(g^3 - 3gt^2 + 2t^3 \cos 2\gamma). \quad (112)$$

This condition singles out all permutation-invariant shared states and is the equation for the boundary surface at  $t_1 = t_2 = t_3$ . Although we have considered shared states for a given  $\gamma$  so far, Eq. (112) shows that there is a single set of shared states and a unique boundary surface separating different subspaces. To complete the picture, we fix other parameters and vary the phase in this section.

In terms of the variables  $(u, v)$ , Eq. (112) imposes a condition on the three angles  $u, v$  and  $\gamma$ . Consequently, knowing two of them, one can find the third angle (provided Eq. (112) admits a solution) at which the state becomes shared. In particular, we will fix a pair  $u, v$  and consider the phase dependence of the maximal overlap. Additionally, we will mark the phase at which the state

<sup>2</sup> This choice means that if the eigenvalues coincide, then the Lagrange multipliers should also coincide. See the proof in Ref. 30.

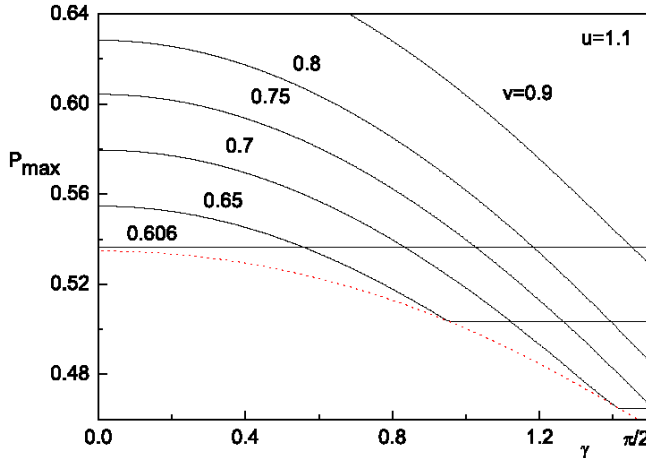


Fig. 7. (Color online) The solid lines are plots of the  $\gamma$ -dependence of  $P_{max}$  when  $u = 1.1$  and  $v = 0.606, 0.65, 0.7, 0.75, 0.8, 0.9$ . The dotted line is the set of shared states for  $u = 1.1$ . When  $v = 0.65$  and  $0.7$ ,  $P_{max}$  decreases monotonically until it intersects the dotted line and then remains constant with increasing  $\gamma$ . This fact indicates that the corresponding quantum states move from a type-II domain to a type-I domain at the value of  $\gamma$  for which the state lies on the boundary. When  $v = 0.606, 0.75, 0.8$ , and  $0.9$ ,  $P_{max}$  exhibits either constant or strictly decreasing behavior everywhere. This fact indicates that the corresponding quantum states stay in one of the applicable domains over the full-range of  $\gamma$ .

becomes shared. That should allow us to see how the state is moving from one to another subspace by passing the boundary surface when  $\gamma$  is increasing.

The first issue we would like to explore is about the number of applicable domains. From the fact that there are two domains each at  $\gamma = 0$  and  $\gamma = \pi/4$ , and three domains at  $\gamma = \pi/2$ , one can naturally conjecture the existence of a critical  $\gamma$ , say  $\gamma_c$ , such that there are two domains for  $\gamma < \gamma_c$  and three domains for  $\gamma > \gamma_c$ . In order to conjecture  $\gamma_c$ , therefore, we have checked the number of domains numerically at  $\gamma = \pi/3$  and  $\gamma = 11\pi/24$ , which also give two applicable domains. From this fact, we have concluded that  $\gamma_c = \pi/2$ , the endpoint of  $\gamma$ . The reason for the emergence of the new domain at  $\gamma = \pi/2$  can be explained as follows: When  $\gamma \neq \pi/2$ , there is only one W state in the  $(u, v)$ -plane at  $u = v = \pi/2$ . When, however,  $\gamma = \pi/2$ , there are two local-unitary equivalent W states in the  $(u, v)$ -plane, one each at  $(u = v = \pi/2)$  and  $(u = \cos^{-1} \sqrt{2}/3, v = \tan^{-1} \sqrt{3}/2)$ . The latter point corresponds to the point in the  $(u, v)$ -plane where the three applicable domains meet. Thus, many highly entangled states congregate around the two points  $(u = v = \pi/2)$  and  $(u = \cos^{-1} \sqrt{2}/3, v = \tan^{-1} \sqrt{3}/2)$ , which forms a new applicable domain in the right-upper corner in the  $(u, v)$ -plane.

The second issue we would like to discuss is about the characteristics of the applicable domains. As mentioned above, there are two applicable domains when

$0 \leq \gamma < \pi/2$ . It is convenient to name these domains for further discussion. One of the domains, which we will call the type-I domain, is located in the left-upper corner in the  $(u, v)$ -plane. For the quantum states that belong to this domain,  $P_{max}$  becomes  $\gamma$  independent. The applicable domains  $P_{max} = \mu_P^2$  for the  $\gamma = 0$  case and  $P_{max} = \rho_P^2$  for the  $\gamma = \pi/4$  case are type-I domain. The other domain, which we will call a type-II domain, spreads out widely in the  $(u, v)$ -plane, except the left-upper corner. The domains  $P_{max} = \mu_+^2$  for the  $\gamma = 0$  case and  $P_{max} = \rho_+^2$  for the  $\gamma = \pi/4$  case are type-II domain. Numerical calculations show that  $P_{max}$  for the quantum states that belong to type-II domains exhibit a monotonically decreasing behavior with increasing  $\gamma$ . This fact implies that the phase factor generally increases the entanglement of the quantum states. Numerical calculations show that the type-I domain expands its range slightly with increasing  $\gamma$ .

We plot the  $\gamma$ -dependence of  $P_{max}$  for several values of  $(u, v)$  in Fig. 7. In order to support our numerical analysis, it is more appealing to choose  $(u, v)$  to be near the boundary of the domains. For this reason, we choose  $u = 1.1$  and  $v = 0.606, 0.65, 0.7, 0.75, 0.8, 0.9$ . When  $v = 0.606$ ,  $P_{max}$  becomes  $\gamma$ -independent. This means that the quantum states corresponding to  $(u = 1, 1, v = 0.606)$  belong to the type-I domain over the full-range of  $\gamma$ . When  $v = 0.75, 0.8$ , and  $0.9$ ,  $P_{max}$  exhibit a monotonically decreasing behavior with increasing  $\gamma$ . This fact implies that the corresponding quantum states belong to a type-II domain over the full-range of  $\gamma$ . When  $v = 0.65$  and  $0.7$ ,  $P_{max}$  exhibits both a monotonically decreasing and a  $\gamma$ -independent behavior. This fact indicates that the corresponding quantum states belong to a type-II domain or a type-I domain, depending on  $\gamma$ . This occurs due to the expansion of the type-I domain with increasing  $\gamma$ .

### VIII. CONCLUSION

In this paper, we have explored the effect of the phase factor in the geometric entanglement measure. We have chosen the most general three-qubit states that have symmetry under qubit-exchange. Our choice of the quantum states enables us to derive all eigenvalues and geometric measures analytically when the phase factor  $\gamma$  is either 0 or  $\pi/2$ . It turns out that the  $\gamma = \pi/2$  case has three applicable domains while the  $\gamma = 0$  case has two domains. Most highly entangled states reside around the boundaries of the domains and near the W state. Apart from the boundaries more and more, quantum states lose their entanglement and eventually become product states.

Our result naturally gives rise to a question: what is the critical  $\gamma$ , say  $\gamma_c$ , that distinguishes the two and three domains? In order to explore this question, we have analyzed the  $\gamma = \pi/4$  case numerically. Our numerical

calculation shows that there are six different eigenvalues for the  $\gamma = \pi/4$  case, but only two of them contribute to the geometric entanglement measure. Thus, there are two domains for  $\gamma = \pi/4$ .

In order to determine  $\gamma_c$  we have examined numerically the number of applicable domains for various  $\gamma$ , all of which give two applicable domains. We also checked the applicable domains for the asymmetric quantum state

$$t_1 = t_2 \neq t_3 \quad (113)$$

numerically when  $\gamma = 0$ . This case also gives two applicable domains. Therefore, we conclude  $\gamma_c = \pi/2$ , the endpoint of the phase factor. The reason for the appearance of a new applicable domain at  $\gamma = \pi/2$  can be explained as follows: Unlike other cases, there are two local-unitary equivalent W states at  $\gamma = \pi/2$  at  $(u = v = \pi/2)$  and  $(u = \cos^{-1}\sqrt{2}/3, v = \tan^{-1}\sqrt{3}/2)$ . Therefore, many highly-entangled states congregate between these two W states. This allows formation of a new applicable domain between two W-states, which is  $P_{max} = \nu_2^2$ .

We have also examined the  $\gamma$ -dependence of  $P_{max}$  for various quantum states. Our numerical calculation shows the following: If the quantum state belongs to a type-I domain, its  $P_{max}$  is  $\gamma$  independent. If, however, the quantum state belongs to a type-II domain, its  $P_{max}$  exhibits a monotonically decreasing behavior with increasing  $\gamma$ . This means that for states belonging to type-II domain, the phase factor generally enhances their entanglement. The main conclusions can be stated in a simple form that there are three different types of pure three-qubit states:

- (i) States belonging to the first subspace: Entanglement of these states does not depend on the phase.
- (ii) States belonging to the second subspace: Entanglement of these states increases with the phase.
- (iii) States belonging to the boundary: These states separate type-I and type-II domains, and depending on the phase, split up the parameter space into either two or three subspaces. All the maximally entangled states [30] and states that allow perfect teleportation and superdense coding [22] are subsets of the shared quantum states. We know precisely among the shared states which ones can be treated as maximally entangled. However, we need to clarify among the shared states those specific states that can be used as a quantum channel for perfect teleportation and superdense coding.

In the appendix, we have shown that there exist eigenvalues for all  $\gamma$ , whose Lagrangian multiplier constant is zero. Although we conjecture that this is due to some symmetry of the quantum state  $|\psi\rangle$ , we do not know the exact physical reason for the emergence of these solutions. It would be of interest to reveal the physical meaning of these solutions clearly.

## ACKNOWLEDGMENTS

This work was supported by the Kyungnam University research fund, 2011.

## APPENDIX A

In this appendix, we would like to show the existence of the eigenvalue  $\mu_0^2$ , which corresponds to  $\lambda = 0$ , at arbitrary  $\gamma$ . When  $\lambda = 0$ , Eq. (14) reduces to

$$2ht \cos \gamma(1 - \cos \theta) + 2t(g + t) \sin \theta \cos \varphi = 0, \quad (A1a)$$

$$2ht \sin \gamma(1 - \cos \theta) - 2t(g - t) \sin \theta \sin \varphi = 0, \quad (A1b)$$

$$(g^2 - t^2)(1 + \cos \theta) - h^2(1 - \cos \theta) - 2ht \sin \theta \cos(\varphi - \gamma) = 0. \quad (A1c)$$

The existence of  $\mu_0^2$  can be shown as follows: First, we derive  $\theta$  and  $\varphi$  by making use of Eq. (A1a) and Eq. (A1b). Then, we show that the solutions  $\theta$  and  $\varphi$  also solve Eq. (A1c).

Now, we consider only the  $\sin \theta \neq 0$  case. Then, from Eq. (A1a) and Eq. (A1b), it is easy to derive

$$(g + t) \sin \gamma \cos \varphi + (g - t) \cos \gamma \sin \varphi = 0, \quad (A2)$$

which gives

$$\tan \varphi = -\frac{g + t}{g - t} \tan \gamma. \quad (A3)$$

Combining Eq. (A2) and Eq. (A3), one can derive the solution for  $\varphi$ , which is

$$\begin{aligned} \cos \varphi &= \pm \frac{g - t}{\sqrt{(g - t)^2 + (g + t)^2 \tan^2 \gamma}}, \\ \sin \varphi &= \mp \frac{(g + t) \tan \gamma}{\sqrt{(g - t)^2 + (g + t)^2 \tan^2 \gamma}}. \end{aligned} \quad (A4)$$

Inserting Eq. (A4) into Eq. (A1b), one can derive  $\sin \theta$  in the form

$$\sin \theta = \mp \frac{2h(g^2 - t^2)\sqrt{g^2 + t^2 - 2gt \cos 2\gamma}}{h^2(g^2 + t^2 - 2gt \cos 2\gamma) + (g^2 - t^2)^2}. \quad (A5)$$

Inserting Eq. (A4) and Eq. (A5) into the lhs of Eq. (A1c), one can show straightforwardly that Eq. (A1c) is solved already by Eq. (A4) and Eq. (A5). This guarantees the existence of  $\mu_0^2$ .

In order to derive  $\mu_0^2$  explicitly, we choose the upper sign in Eq. (A4) and in Eq. (A5). Then, the components of the vector  $s$  become

$$s_x = \sin \theta \cos \varphi = \frac{-2h(g - t)^2(g + t) \cos \gamma}{h^2[(g^2 + t^2) - 2gt \cos 2\gamma] + (g^2 - t^2)^2},$$

(A6a)

$$s_y = \sin \theta \sin \varphi = \frac{2h(g-t)(g+t)^2 \sin \gamma}{h^2[(g^2+t^2)-2gt \cos 2\gamma] + (g^2-t^2)^2}, \quad (A6b)$$

$$s_z = \cos \theta = \frac{h^2[(g^2+t^2)-2gt \cos 2\gamma] - (g^2-t^2)^2}{h^2[(g^2+t^2)-2gt \cos 2\gamma] + (g^2-t^2)^2}. \quad (A6c)$$

Inserting Eq. (A6) into Eq. (8) and performing tedious calculations, one can show that  $\mu_0^2$ , the eigenvalue corresponding to  $\lambda = 0$ , becomes

$$\mu_0^2 = \frac{g^2 h^2 (g^2 + t^2 - 2gt \cos 2\gamma) + t^2 (g^2 - t^2)^2}{h^2 (g^2 + t^2 - 2gt \cos 2\gamma) + (g^2 - t^2)^2}. \quad (A7)$$

It is straightforward to show that the choice of the lower sign in Eq. (A4) and in Eq. (A5) leads us to the same expression for  $\mu_0^2$ . One can show easily that  $\mu_0^2$  exactly coincides with  $\mu_1^2$  in Eq. (25),  $\nu_1^2$  in Eq. (43) and  $\rho_0^2$  in Eq. (111) when  $\gamma = 0$ ,  $\gamma = \pi/2$ , and  $\gamma = \pi/4$ , respectively.

Finally, making use of the explicit expression for  $\mu_0^2$ , one can derive the nearest product state  $|q\rangle|q'\rangle|q'\rangle$  for  $\mu_0^2$ , i.e.,

$$\begin{aligned} AB\langle q|\langle q|\psi\rangle &= \mu_0|q'\rangle, & AC\langle q|\langle q'|\psi\rangle &= \mu_0|q\rangle, \\ BC\langle q|\langle q'|\psi\rangle &= \mu_0|q\rangle, \end{aligned} \quad (A8)$$

where  $|\psi\rangle$  is given in Eq. (7). Since  $s$  is a Bloch vector of  $|q\rangle\langle q|$ , one can show directly that

$$|q\rangle = \frac{1}{\sqrt{h^2\ell^2 + (g^2 - t^2)^2}} [h\ell|0\rangle - (g^2 - t^2)e^{-i\eta}|1\rangle], \quad (A9)$$

where

$$\begin{aligned} \ell^2 &\equiv g^2 + t^2 - 2gt \cos 2\gamma, & \cos \eta &= \frac{g - t}{\ell} \cos \gamma, \\ \sin \eta &= \frac{g + t}{\ell} \sin \gamma. \end{aligned} \quad (A10)$$

Inserting Eq. (A9) into Eq. (A8), it is straightforward to show that  $|q'\rangle$  becomes

$$\begin{aligned} |q'\rangle &= \frac{1}{\mathcal{N}} [\{gh^2\ell^2 + t(g^2 - t^2)^2 e^{2i\eta}\}|0\rangle \\ &\quad + e^{i\eta}h(g^2 - t^2)\{(g^2 - t^2)e^{i(\gamma+\eta)} - 2\ell t\}|1\rangle], \end{aligned} \quad (A11)$$

where  $\mathcal{N}$  is a normalization constant, which makes  $|q'\rangle$  a unit vector.

For the  $\gamma = 0$  case, the nearest product state becomes

$$|q\rangle = \frac{1}{\sqrt{h^2 + (g+t)^2}} (h|0\rangle - (g+t)|1\rangle), \quad (A12)$$

$$|q'\rangle = \frac{1}{\sqrt{\{gh^2 + t(g+t)^2\}^2 + h^2(g^2 - t^2)^2}}$$

$$\times [\{gh^2 + t(g+t)^2\}|0\rangle + h(g^2 - t^2)|1\rangle]. \quad (A13)$$

It is interesting to note that  $\langle q|q'\rangle = 0$  when  $\mathcal{D}_1 = 0$ , where  $\mathcal{D}_1$  is given in Eq. (63).

For the  $\gamma = \pi/2$  case,  $|q\rangle$  abd  $|q'\rangle$  becomes

$$|q\rangle = \frac{1}{\sqrt{h^2 + (g-t)^2}} (h|0\rangle + i(g-t)|1\rangle), \quad (A14)$$

$$\begin{aligned} |q'\rangle &= \frac{1}{\sqrt{\{gh^2 - t(g-t)^2\}^2 + h^2(g^2 - t^2)^2}} \\ &\times [\{gh^2 - t(g-t)^2\}|0\rangle - ih(g^2 - t^2)|1\rangle]. \end{aligned} \quad (A15)$$

It is interesting to note that  $\langle q|q'\rangle = 0$  when  $\mathcal{C}_3 = 0$ , where  $\mathcal{C}_3$  is given in Eq. (89).

## REFERENCES

- [1] R. F. Werner, Phys. Rev. A **40**, 4277 (1989).
- [2] A. K. Ekert, Phys. Rev. Lett. **67**, 661 (1991).
- [3] C. H. Bennett and S. J. Wiesner, Phys. Rev. Lett. **69**, 2881 (1992).
- [4] C. H. Bennett, G. Brassard, C. Crépeau, R. Jozsa, A. Peres and W. K. Wootters, Phys. Rev. Lett. **70**, 1895 (1993).
- [5] F. Casagrande, A. Lulli and M. G. A. Paris, Phys. Rev. A **79**, 022307 (2009).
- [6] C. H. Bennett, H. J. Bernstein, S. Popescu and B. Schumacher, Phys. Rev. A **53**, 2046 (1996).
- [7] C. H. Bennett, D. P. DiVincenzo, J. A. Smolin and W. K. Wootters, Phys. Rev. A **54**, 3824 (1996).
- [8] W. K. Wootters, Phys. Rev. Lett. **80**, 2245 (1998).
- [9] G. Vidal and J. I. Cirac, Phys. Rev. Lett. **86**, 5803 (2001).
- [10] V. Vedral, M. B. Plenio, M. A. Rippin and P. L. Knight, Phys. Rev. Lett. **78**, 2275 (1997).
- [11] M. B. Plenio and V. Vedral, J. Phys. A: Math. Gen. **34**, 6997 (2001).
- [12] D. A. Meyer and N. R. Wallach, J. Math. Phys. **43**, 4273 (2002).
- [13] O. Biham, M. A. Nielsen and T. J. Osborne, Phys. Rev. A **65**, 062312 (2002).
- [14] D. Shapira, Y. Shimoni and O. Biham, Phys. Rev. A **73**, 044301 (2006).
- [15] A. Shimony, Ann. N.Y. Acad. Sci. **755**, 675 (1995).
- [16] H. Barnum and N. Linden, J. Phys. A: Math. Gen. **34**, 6787 (2001).
- [17] T. C. Wei and P. M. Goldbart, Phys. Rev. A **68**, 042307 (2003).
- [18] R. Werner and A. Holevo, J. Math. Phys. **43**, 4353 (2002).
- [19] L. Tamaryan, D. K. Park and S. Tamaryan, ArXiv:0809.1290 (quant-ph).
- [20] J. J. Hilling and A. Sudbery, J. Math. Phys. **51**, 072102 (2010).
- [21] L. Tamaryan, D. K. Park and S. Tamaryan, Phys. Rev. A **77**, 022325 (2008).
- [22] L. Tamaryan, D. K. Park, J. W. Son and S. Tamaryan, Phys. Rev. A **78**, 032304 (2008).
- [23] E. Jung, M. R. Hwang, D. K. Park, L. Tamaryan and S. Tamaryan, Quantum Inf. Comput. **8**, 0925 (2008).

- [24] Y. Shimonini, D. Shapira and O. Biham, Phys. Rev. A **69**, 062303 (2004).
- [25] M. Hayashi, D. Markham, M. Murao, M. Owari and S. Virmani, Phys. Rev. Lett. **96**, 040501 (2006).
- [26] O. Gühne, F. Bodoky and M. Blaauboer, Phys. Rev. A **78**, 060301(R) (2008).
- [27] L. Tamaryan, H. Kim, E. Jung, M. R. Hwang, D. K. Park and S. Tamaryan, J. Phys. A: Math. Theor. **42**, 475303 (2009).
- [28] H. A. Carteret, A. Higuchi and A. Sudbery, J. Math. Phys. **41**, 7932 (2000).
- [29] A. Acín, A. Andrianov, L. Costa, E. Jané, J. I. Latorre and R. Tarrach, Phys. Rev. Lett. **85**, 1560 (2000).
- [30] S. Tamaryan, T. C. Wei and D. K. Park, Phys. Rev. A **80**, 052315 (2009).
- [31] W. Dür, G. Vidal and J. I. Cirac, Phys. Rev. A **62**, 062314 (2000).
- [32] S. J. van Enk, Phys. Rev. Lett. **102**, 190503 (2009).
- [33] G. Toth and O. Gühne, Phys. Rev. Lett. **102**, 170503 (2009).
- [34] T. C. Wei and S. Severini, J. Math. Phys. **51**, 092203 (2010).